



# **Robot-Assisted Endodontic Treatment**

*Yi-Chan Li*

*Advisor: Cheng-Wei Chen*

*Graduate Institute of Electronics Engineering*

*National Taiwan University*

*Taipei, Taiwan*

June 2021

# **Abstract**

1.introduction: present tense

2.method and result: past tense

3.conclusion : present tense



# Contents

<b>Abstract</b>	<b>i</b>
<b>List of Figures</b>	<b>vii</b>
<b>List of Tables</b>	<b>ix</b>
<b>1 Introduction</b>	<b>1</b>
1.1 Motivation . . . . .	1
1.2 Previous Work and Problem Definition . . . . .	2
1.3 The Proposed Method . . . . .	5
1.4 Main Contributions of the Thesis . . . . .	6
1.5 Organization of the Thesis . . . . .	6
<b>2 State-of-the-Art</b>	<b>7</b>
<b>3 Design and Analysis of the Dental Surgical Robot - DentiBot</b>	<b>9</b>
3.1 Requirement and Specification . . . . .	9
3.2 Design of the DentiBot . . . . .	10

3.3	Kinematics Analysis . . . . .	11
3.3.1	Coordinate Definition . . . . .	11
3.3.2	Forward and Inverse Kinematics . . . . .	13
3.3.3	Jacobian matrix . . . . .	14
3.4	Coordinate Transformation of the Robot Arm . . . . .	20
3.4.1	Translation Analysis - Tool Center Point . . . . .	21
3.4.2	Rotation Analysis . . . . .	24
<b>4</b>	<b>Force-Guided Robot Alignment</b>	<b>27</b>
4.1	Problem Definition . . . . .	28
4.2	Integration of F/T sensor . . . . .	29
4.3	Dragging Mode . . . . .	37
4.3.1	Admittance Control based on F/T sensor . . . . .	38
4.4	Self-Alignment Mode . . . . .	42
4.4.1	Coordinate Transformation of F/T sensor . . . . .	43
4.4.2	Motion Planning: Based on Admittance Control . . . . .	45
4.5	Affections of Parameters Setting . . . . .	46
<b>5</b>	<b>Control of Endodontic File Rotation</b>	<b>51</b>
5.1	Problem Definition . . . . .	51
5.2	The Proposed Method and Theorem . . . . .	51
<b>6</b>	<b>Preliminary Experiment Result</b>	<b>53</b>
6.1	Experimental Setup . . . . .	53

<i>CONTENTS</i>	v
6.2 Admittance Control . . . . .	53
6.3 Automatically Direction Changing . . . . .	54
6.4 Repetitive Experiment . . . . .	54
<b>7 Conclusions and Future works</b>	<b>55</b>
<b>8 Appendix</b>	<b>57</b>
8.1 Forward Kinematics . . . . .	57
8.2 Jacobian matrix . . . . .	60
8.2.1 $J_{g0}$ . . . . .	60
8.2.2 $J_{g6}$ . . . . .	63
<b>Reference</b>	<b>65</b>





# List of Figures

1.1	The endodontic therapy steps . . . . .	3
3.1	Workspace of Meca500 . . . . .	11
3.2	Coordinate Definition . . . . .	12
3.3	Schematic diagram for Tool Center Point. The translation vector ${}^6\mathbf{p}_{\text{Horg}}$ denotes the origin position relative to the frame{6}. . . . .	22
3.4	Schematic diagram for obtaining the tool vector. . . . .	24
3.5	Illustration of finding the rotation matrix . . . . .	25
4.1	Data Analysis of F/T sensor. . . . .	29
4.2	Control scheme. $\mathbf{f}_d$ denotes the desired forces and torques vector. $\mathbf{f}_s$ denotes the real value detected by F/T sensor and is also a forces and torques vector. $\dot{\mathbf{x}}$ denotes $[\dot{x}, \dot{y}, \dot{z}, \dot{\theta}_x, \dot{\theta}_y, \dot{\theta}_z]$ . $\mathbf{J}_g$ denotes the geometric Jacobian matrix. $\dot{\mathbf{q}}$ denotes $[\dot{\theta}_1, \dot{\theta}_2, \dot{\theta}_3, \dot{\theta}_4, \dot{\theta}_5, \dot{\theta}_6]$ . $\mathbf{q}$ denotes $[\theta_1, \theta_2, \theta_3, \theta_4, \theta_5, \theta_6]$ . . . . .	38
4.3	Illustration of changing reference frame from {S} to {T}. $\mathbf{f}$ and $\mathbf{m}$ respectively denote a force and a moment measured at point p. . .	43

4.4	Illustration of changing reference frame from $\{S\}$ to $\{T\}$ . $\mathbf{f}$ and $\mathbf{m}$ respectively denote a force and a moment measured at point $p$ .	44
4.5	Flow chart of motion planning . . . . .	46
4.6	Flow chart of motion planning . . . . .	47
4.7	Control scheme. $\mathbf{M}$ , $\mathbf{B}$ , $\mathbf{K}$ are all diagonal positive definite matrices, whose diagonal indexes are respectively related to $x, y, z, \theta_x, \theta_y, \theta_z$ . $\mathbf{M}$ , $\mathbf{B}$ are related to the inertial and damping respectively, and $\mathbf{K}$ is a proportional gain. . . . .	47
4.8	Holding gesture in "Dragging Mode" . . . . .	50

# List of Tables

3.1	Denavit-Hartenberg parameters of Meca500 . . . . .	13
4.1	Arc-function Comparison . . . . .	36
4.2	Moving commands in Meca500 . . . . .	40
4.3	Parameters setting of Admittance control. . . . .	49



# Chapter 1

## Introduction

The robot-assisted system for endodontic treatment - DentiBot is presented in this thesis. The definition of a robot-assisted system in the thesis refers to be a dental assistant. That means we wish DentiBot could help dentists perform better clinical results. This chapter will give brief introductions of the endodontic treatment, previous work, problem definition, and the proposed method.

### 1.1 Motivation

A qualified dentist can operate an endodontic treatment. They accumulate their experience, thereby increasing the success rate. With enough clinical experience, the dentist can acquire an endodontist license. According to statistics from the Ministry of Health and Welfare, R.O.C. (Taiwan) [1], the number of dentists in Taiwan is 15,178. However, according to The Academy of Endodontology, R.O.C. (Taiwan) [2], there are only 238 dentists to acquire an endodontist license.

Thus, performing an endodontic treatment requires the dentist's self expertise of endodontics. The performance of endodontic treatment depends on a dentist's long-term experience.

Besides, root canal treatment is a tedious and time-consuming surgery for a dentist due to the different complicated conditions of each tooth. A patient who suffered from an infected tooth spends countless hours see a dentist. It takes at least two to three rounds of treatments, even more than two months in the worst case.

Therefore, our team looks forward to designing a robot-assisted system to accomplish a root canal treatment. With the robot, we wish it can reduce times for entire treatment, increase the success rate of root canal treatment for dentists, and provide patients safer surgery.

## 1.2 Previous Work and Problem Definition

First, we introduce the endodontic treatment and its detailed procedure.

*Endodontic treatment*, also known as root canal treatment and nerve extraction, is performed to cure an infected tooth. The main procedure of endodontic treatment is divided into three parts - Opening, Cleaning, and Filling shown in Figure 1.1.

An infected tooth arises from periodontal disease, attrition, trauma, or decay. Once the dental pulp is infected, it causes an irreversible inflammation and lets patients confront a root canal treatment. Figure 1.1 shows an infected tooth and its dental pulp, which consisted of blood vessels, nerves, connective tissues, and

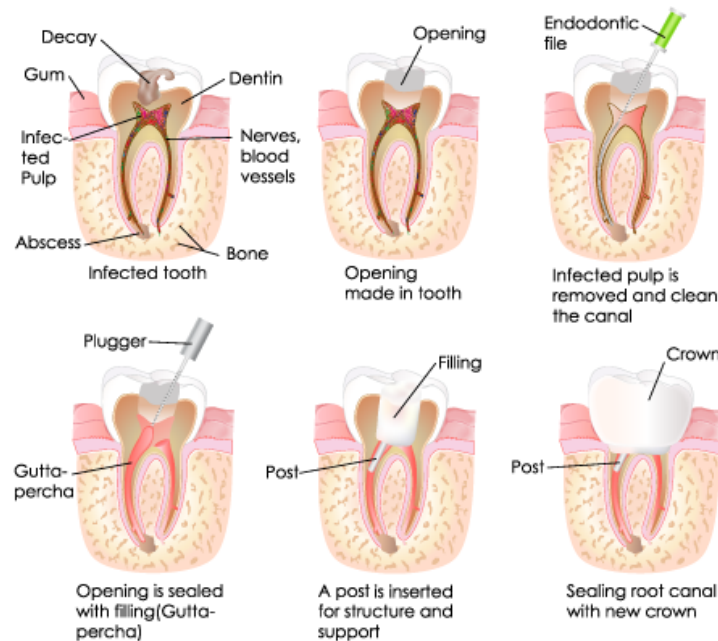


Figure 1.1: The endodontic therapy steps

lymphatics. In the "Opening" step, an experienced dentist drills the crown of the infected tooth to remove the dentin and expose the infected pulp inside the canal to the air. Next, in the "Cleaning" step, the dentist uses an endodontic file, a superelastic root reamer, to remove the infected pulp. It is necessary to ensure that there is no remained infected pulp. Then, in the "Filling" step, the dentist uses a dental plugger to fill the empty root canal with Gutta-percha, a plastic substance. "Filling" can prevent cross-infection between root canals because the cured tooth remains many invisible and inaccessible pulp tissue. Finally, the dentist seals the root canal with a new crown to protect cured root canal.

As stated above, "Cleaning" is of paramount importance in a whole treatment because cleaning improperly will result in pulp necrosis, apical abscess, periodontal

ligament inflammation, or even cellulitis. If there are many remained infected pulp after root canal treatment, the surgery should be operated on again. The "Cleaning" procedure is a big challenge in and of itself. Therefore, we should figure out how to enable the robot to assist dentists and perform the root canal treatment.

There are more and more robots which applied to specific surgery. In the dental field, the majority of robotic applications are in implant surgery. The researchers in Chosun University built a dental implant robot [3], a remote center of motion (RCM) mechanism. Li, J. et al. designed a robotic system using a soft bracing technique to drill teeth [4]. Also, there is the first commercial implant robot, YOMI, developed by Neosis [5]. However, there was one and only one robot for the endodontic treatment. The domestic researcher Janet Dong and his team proposed a microrobot performing root canal treatment with the assistance of a 3D computer model system. However, the study using 3D model belongs to pre-operation. If a patient or an image error causes a movement, it will not be easy to reschedule the motion planning because the root canal in a tooth is unseen by a camera from any angle. Besides, once an endodontic file enters into a root canal, it is hard to obtain the tool tip position due to its flexibility. The endodontic file will bend when it bears a force. Once we lose the position of the endodontic file, it may lead to perforation, overpreparation, and underpreparation. Therefore, a problem reveals - how the robot know the path of a root canal without visual feedback?

On the other hand, instrument fracture is the other concern during the therapy. If an endodontic file suffered excessive usage, it would unpredictably break. The



leading causes of fractured files are torsional fracture and flexural fatigue, which account for 55.7% and 44.3% separately [6]. Removal of broken files is technically tricky, so it is essential to reduce the probability of the instrument fracture. Therefore, our robot should prevent the instrument fracture by some detection. In addition, the root canal treatment also requires repeatedly drilling to clean the canal thoroughly and motion planning to avoid perforation. This repetitive action of root canal treatment is tedious and time-consuming. Therefore, we decide to design an automatic endodontic robot. It can improve time efficiency and prevent instrument fracture in endodontic treatment.

To sum up, there are three main problem definition.

1. How to assist dentists to perform the root canal treatment including motion planning, especially in the second procedure - cleaning?
2. How to overcome the problem that the root canal cannot be visually observed, and how to clean well in any complex conditions?
3. How to protect the endodontic file from fracturing during the surgery?

## **1.3 The Proposed Method**

To assist dentists in accomplishing an endodontic treatment, we build a robot - DentiBot to provide more precise and safer treatment. DentiBot consists of a robot arm, a force/torque sensor, and a modified end effector. With the robot arm, we could make the system manifest various motions such as reciprocation; with the

force/torque sensor, we could align the root canal path by force feedback. And with the modified handpiece, a handheld dental electric device, it satisfied the workspace of dental surgery. 1. Build a robot-assisted system and enable it to drill 2. Force-guided alignment 3. Control the file rotation speed we use current feedback to keep track of the file's torque during the endodontic treatment. *Prospect:* There are four parts of the robot-assisted project. First, we wish the robot could move to the infected tooth. That (Prospect: Move to the infected teeth—→Root canal searching—→Repetitive drilling—→Apex Detection)

## 1.4 Main Contributions of the Thesis

In conclusion, there are three main contributions the thesis make.

1. Integrate a 6-DoF robotic manipulator with 6-DoF F/T sensor for performing endodontic treatment.
2. Develop a framework for robot alignment regarding the position and orientation of root canal.
3. Protect the endodontic file from fracturing by controlling file rotation speed.

## 1.5 Organization of the Thesis

The structure of this thesis is as follows.

## **Chapter 2**

### **State-of-the-Art**

A. YOMI – commercial robot B. HK - dental implant robot C. Korean - dental implant robot D. NCTU – RCT robot It utilizes the 3D model to plan the corresponding path to accomplish an endodontic treatment. YOMI has received the clearance from FDA and has performed more than 2,700 times surgery in the USA. In the pandemic of Covid-19 in 2020, YOMI provided non-contact surgery between dentists and patients due to its automatic robotic system.



## Chapter 3

# Design and Analysis of the Dental Surgical Robot - DentiBot

### 3.1 Requirement and Specification

(Payload, resolution and workspace) (Why not RCM mechanism)

The dental surgical robot should enable dentists to perform delicate and complicated surgery operations because the average diameter of a root canal is  $0.28(\pm 0.08)$  mm [7]. Therefore, our system should have a high resolution. Next, an appropriate workspace is required. In dental anatomy, teeth are located on the maxillary (lower jaw) and the mandibular (upper jaw). To perform surgery with both sides, we should rotate the end effector at least 180 degrees. Also, there is previous research, which shows the average range of maximum mouth opening is  $50.3 \text{ mm} \pm 6.26 \text{ mm}$  [8]. Hence, the end effector of our system should be less than the range. To achieve

the workspace, we build a system composed of a robot arm, an F/T sensor, and a modified handpiece. We choose a robot arm and an F/T sensor because we want to mimic the dentist's motion. Due to six degrees of freedom (DOF) with the robot arm and the F/T sensor, we can achieve the action with less hardware restriction. Besides, by modifying the existing handpiece, which is a dental instrument for oral surgery, we do not worry about the workspace in the mouth.

## **3.2 Design of the DentiBot**

As discussed in the previous section, we have to select suitable devices according to those requirements. First, We choose Meca500 manufactured by Mecademic Inc. as our 6 DOF robot arm. Its feature is high repeatability (precision: 5  $\mu\text{m}$ ), and it is equipped with zero-backlash speed reducers. In addition, it is compact and portable for laboratory investigation. Second, Mini40 manufactured by ATI Inc. is the corresponding F/T sensor with three force and three torque detections. As for the end effector, we modify an existing dental handpiece that equips a tool change mechanism. The modified handpiece weighs around 139 grams. We also design adapters to assemble these devices.

DentiBot has seven degrees of freedom. 6 DOF comes from Meca500, and the other DOF is owing to our modified handpiece. The rotation of the root canal file is driven by a servo motor whose maximum rotation speed is more than 600 rpm.

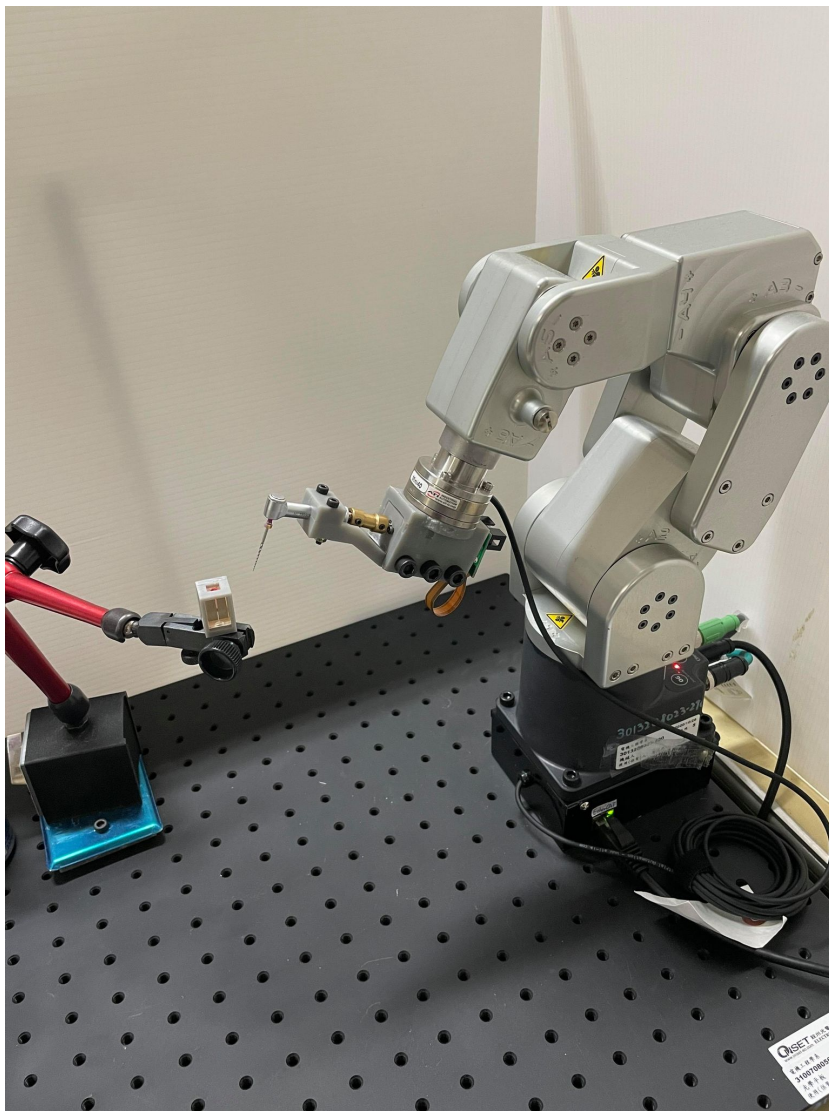


Figure 3.1: The DentiBot and an acyclic tooth model

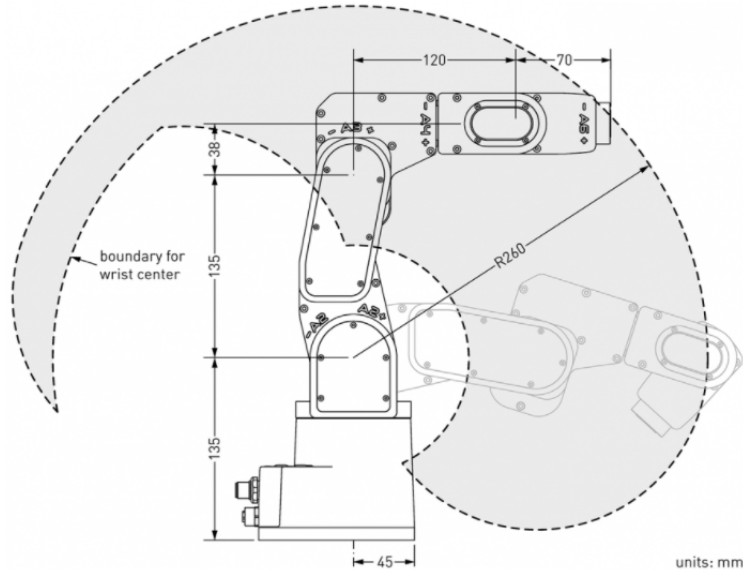


Figure 3.2: Workspace of Meca500

### 3.3 Kinematics Analysis

The purpose of this section and section 3.4 is to serve as a tutorial and provide some crucial approaches when combining a robot arm and an end effector. We derive the forward and inverse kinematics in section 3.3.2 and describe the Jacobian matrix in section 3.3.3.

#### 3.3.1 Coordinate Definition

In Fig 3.2 , we define frame{0} to frame{6} which represent each frame of axes of the Meca500, frame{S} which represent the frame of the ATI-mini40 and frame{H} which represent the frame of the handpiece.



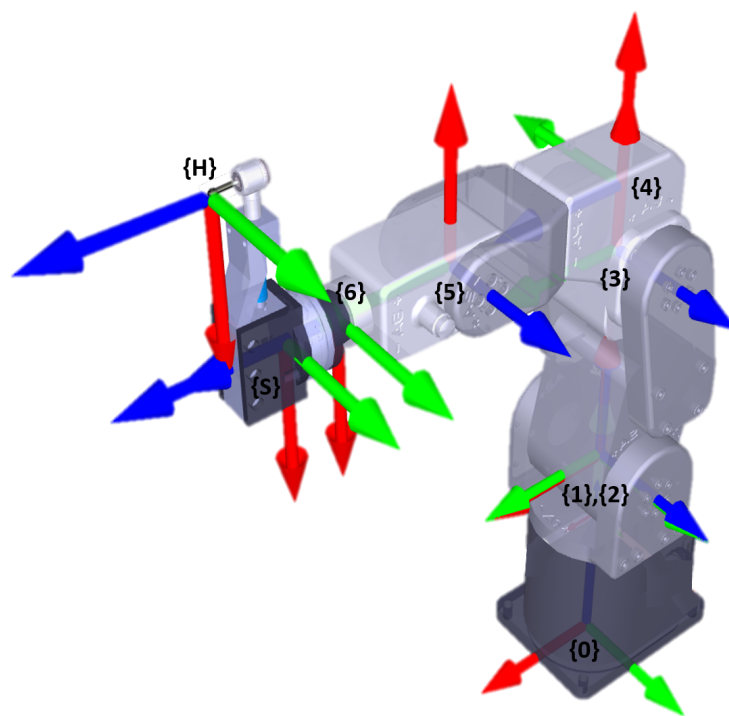


Figure 3.3: Coordinate Definition

### 3.3.2 Forward and Inverse Kinematics

Table 3.1: Denavit-Hartenberg parameters of Meca500

$i$ (link number)	$\alpha_{i-1}$ (deg)	$a_{i-1}$ (mm)	$\theta_i$ (deg)	$d_i$ (mm)
1	0	0	$\theta_1$	135
2	-90	0	$\theta_2$	0
3	0	135	$\theta_3$	0
4	-90	38	$\theta_4$	120
5	90	0	$\theta_5$	0
6	-90	0	$\theta_6$	70

Denavit-Hartenberg parameters are shown as Table 3.1. Then, the forward kinematics of Meca500 is derived as

$${}^0_6\mathbf{T} = {}^0_1\mathbf{T} \cdot {}^1_2\mathbf{T} \cdot {}^2_3\mathbf{T} \cdot {}^3_4\mathbf{T} \cdot {}^4_5\mathbf{T} \cdot {}^5_6\mathbf{T} = \begin{bmatrix} {}^0_6\mathbf{R} & {}^0\mathbf{p}_{6\text{org}} \\ 0 & 1 \end{bmatrix} \quad (3.1)$$

where  ${}^0_6\mathbf{R}$  is the rotation matrix from frame{6} to frame{0},  ${}^0\mathbf{p}_{6\text{org}}$  is the origin of the frame{6} observed from frame{0}. All detailed indexes of  ${}^0_6\mathbf{T}$  are shown as Appendix 8.1

Incidentally, there is an alternative to calculate the transformation matrix of Meca500. We can use command "GetPose" to obtain (x,y,z, $\alpha,\beta,\gamma$ ). Then, we can

use this information to derive the following equation.

$$\begin{aligned}
 {}^0_6\mathbf{T} &= \begin{bmatrix} & x \\ \mathbf{R}_x(\alpha) \cdot \mathbf{R}_y(\beta) \cdot \mathbf{R}_z(\gamma) & y \\ & z \\ 0 & 1 \end{bmatrix} \\
 &= \begin{bmatrix} c_\beta c_\gamma & -c_\beta s_\gamma & s_\beta & x \\ c_\alpha s_\gamma + s_\alpha s_\beta c_\gamma & c_\alpha c_\gamma - s_\alpha s_\beta s_\gamma & -s_\alpha c_\beta & y \\ s_\alpha s_\gamma - c_\alpha s_\beta c_\gamma & s_\alpha c_\gamma + c_\alpha s_\beta s_\gamma & c_\alpha c_\beta & z \\ 0 & 0 & 0 & 1 \end{bmatrix} \quad (3.2)
 \end{aligned}$$

where  $C_\star, S_\star$  denote  $\cos(\star), \sin(\star)$ ;  $\alpha, \beta, \gamma$  are in representation of Euler angle.

### 3.3.3 Jacobian matrix

Here we evaluate geometric Jacobian based on frame $\{0\}$ , geometric Jacobian based on frame $\{6\}$  and analytical Jacobian.

First and foremost, we should clarify the difference between geometric Jacobian and analytical Jacobian. They both use the same linear velocity but consider different angular velocity. The angular velocity which geometric Jacobian applies is relevant to the axis angles  $(\theta_x, \theta_y, \theta_z)$ . In contrast, the angular velocity which analytical Jacobian contemplates is related to the orientation  $(\alpha, \beta, \gamma)$  of the end effector.

### Geometric Jacobian Based on Frame{0}

Before examining the geometric Jacobian matrix, it will be necessary to find the relationship between the position and joints' angles and the relationship between the axis angle and the joints' angles.

Based on the translation matrix in Equation 3.3.2, we obtain the relationship between the position and joints' angles.

$${}^0\mathbf{p}_{\text{org}} = \begin{bmatrix} x \\ y \\ z \end{bmatrix} = \begin{bmatrix} x(\theta_1, \theta_2, \dots, \theta_6) \\ y(\theta_1, \theta_2, \dots, \theta_6) \\ z(\theta_1, \theta_2, \dots, \theta_6) \end{bmatrix} \quad (3.3)$$

Moreover, we dissect the relationship between the axis angle and joints' angles.

$$\begin{bmatrix} \theta_x \\ \theta_y \\ \theta_z \end{bmatrix} = {}^0_1\mathbf{R} \begin{bmatrix} 0 \\ 0 \\ \theta_1 \end{bmatrix} + {}^0_2\mathbf{R} \begin{bmatrix} 0 \\ 0 \\ \theta_2 \end{bmatrix} + {}^0_3\mathbf{R} \begin{bmatrix} 0 \\ 0 \\ \theta_3 \end{bmatrix} + {}^0_4\mathbf{R} \begin{bmatrix} 0 \\ 0 \\ \theta_4 \end{bmatrix} + {}^0_5\mathbf{R} \begin{bmatrix} 0 \\ 0 \\ \theta_5 \end{bmatrix} + {}^0_6\mathbf{R} \begin{bmatrix} 0 \\ 0 \\ \theta_6 \end{bmatrix} \quad (3.4)$$

We can differentiate Equation 3.3 and 3.4 to obtain Jacobian matrices.

$$\mathbf{v} = \begin{bmatrix} \dot{x} \\ \dot{y} \\ \dot{z} \end{bmatrix} = \mathbf{J}_{\mathbf{gv}} \cdot \dot{\mathbf{q}}, \quad \mathbf{w} = \begin{bmatrix} \dot{\theta}_x \\ \dot{\theta}_y \\ \dot{\theta}_z \end{bmatrix} = \mathbf{J}_{\mathbf{gw}} \cdot \dot{\mathbf{q}} \quad (3.5)$$

where

$$\mathbf{J}_{\mathbf{gv}} = \begin{bmatrix} \frac{\partial x}{\partial \theta_1} & \frac{\partial x}{\partial \theta_2} & \dots & \frac{\partial x}{\partial \theta_6} \\ \frac{\partial y}{\partial \theta_1} & \frac{\partial y}{\partial \theta_2} & \dots & \frac{\partial y}{\partial \theta_6} \\ \frac{\partial z}{\partial \theta_1} & \frac{\partial z}{\partial \theta_2} & \dots & \frac{\partial z}{\partial \theta_6} \end{bmatrix}, \mathbf{J}_{\mathbf{gw}} = \begin{bmatrix} \frac{\partial \theta_x}{\partial \theta_1} & \frac{\partial \theta_x}{\partial \theta_2} & \dots & \frac{\partial \theta_x}{\partial \theta_6} \\ \frac{\partial \theta_y}{\partial \theta_1} & \frac{\partial \theta_y}{\partial \theta_2} & \dots & \frac{\partial \theta_y}{\partial \theta_6} \\ \frac{\partial \theta_z}{\partial \theta_1} & \frac{\partial \theta_z}{\partial \theta_2} & \dots & \frac{\partial \theta_z}{\partial \theta_6} \end{bmatrix}, \dot{\mathbf{q}} = \begin{bmatrix} \dot{\theta}_1 \\ \dot{\theta}_2 \\ \dot{\theta}_3 \\ \dot{\theta}_4 \\ \dot{\theta}_5 \\ \dot{\theta}_6 \end{bmatrix}$$

As a result, the geometric Jacobian matrix based on frame0  ${}^0\mathbf{J}_{\mathbf{g}}$  is derived as

$$\dot{\mathbf{x}} = {}^0\mathbf{J}_{\mathbf{g}} \cdot \dot{\mathbf{q}}, \quad \dot{\mathbf{q}} = {}^0\mathbf{J}_{\mathbf{g}}^{-1} \cdot \dot{\mathbf{x}} \quad (3.6)$$

where

$$\dot{\mathbf{x}} = \begin{bmatrix} \dot{x} \\ \dot{y} \\ \dot{z} \\ \dot{\theta}_x \\ \dot{\theta}_y \\ \dot{\theta}_z \end{bmatrix}_{\{0\}}, \quad \dot{\mathbf{q}} = \begin{bmatrix} \dot{\theta}_1 \\ \dot{\theta}_2 \\ \dot{\theta}_3 \\ \dot{\theta}_4 \\ \dot{\theta}_5 \\ \dot{\theta}_6 \end{bmatrix} \quad (3.7)$$

There is a further derivation. In terms of the Jacobian matrix, we can derive the

other property.

$$\boldsymbol{\tau} = {}^0\mathbf{J}_g^\top \cdot \mathbf{f} \Leftrightarrow \begin{bmatrix} \tau_{\theta_1} \\ \tau_{\theta_2} \\ \tau_{\theta_3} \\ \tau_{\theta_4} \\ \tau_{\theta_5} \\ \tau_{\theta_6} \end{bmatrix} = {}^0\mathbf{J}_g^\top \cdot \begin{bmatrix} f_x \\ f_y \\ f_z \\ \tau_x \\ \tau_y \\ \tau_z \end{bmatrix} \quad (3.8)$$

where  $\boldsymbol{\tau}$  is the vector of joints' torques and  $\mathbf{f}$  is the vector composed of inertial forces and torques of the robot arm.

### Geometric Jacobian Based on Frame{6}

Why we need geometric Jacobian based on frame{6} is that in section 4.3.1 we will apply admittance control and it will use F/T sensor mounted on frame{6} instead of frame{0} to detect forces and torques. To start with Equation 3.6

$$\begin{bmatrix} \dot{x} \\ \dot{y} \\ \dot{z} \\ \dot{\theta}_x \\ \dot{\theta}_y \\ \dot{\theta}_z \end{bmatrix}_{\{0\}} = {}^0\mathbf{J}_g \cdot \begin{bmatrix} \dot{\theta}_1 \\ \dot{\theta}_2 \\ \dot{\theta}_3 \\ \dot{\theta}_4 \\ \dot{\theta}_5 \\ \dot{\theta}_6 \end{bmatrix} \quad (3.9)$$

Then, left-multiply a matrix.

$$\begin{bmatrix} {}^0_6\mathbf{R} & 0_{3 \times 3} \\ 0_{3 \times 3} & {}^0_6\mathbf{R} \end{bmatrix} \begin{bmatrix} \dot{x} \\ \dot{y} \\ \dot{z} \\ \dot{\theta}_x \\ \dot{\theta}_y \\ \dot{\theta}_z \end{bmatrix}_{\{0\}} = \begin{bmatrix} {}^0_6\mathbf{R} & 0_{3 \times 3} \\ 0_{3 \times 3} & {}^0_6\mathbf{R} \end{bmatrix} {}^0\mathbf{J}_g \cdot \begin{bmatrix} \dot{\theta}_1 \\ \dot{\theta}_2 \\ \dot{\theta}_3 \\ \dot{\theta}_4 \\ \dot{\theta}_5 \\ \dot{\theta}_6 \end{bmatrix} \quad (3.10)$$

According to the transformation coordinate relationship between frame $\{0\}$  and frame $\{6\}$ ,

$$\begin{bmatrix} \dot{x} \\ \dot{y} \\ \dot{z} \\ \dot{\theta}_x \\ \dot{\theta}_y \\ \dot{\theta}_z \end{bmatrix}_{\{6\}} = \begin{bmatrix} {}^0_6\mathbf{R} & 0_{3 \times 3} \\ 0_{3 \times 3} & {}^0_6\mathbf{R} \end{bmatrix} \begin{bmatrix} \dot{x} \\ \dot{y} \\ \dot{z} \\ \dot{\theta}_x \\ \dot{\theta}_y \\ \dot{\theta}_z \end{bmatrix}_{\{0\}} \quad (3.11)$$

substitute it into Eq 3.10, we can observe an essential equation.

$${}^6\mathbf{J}_g = \begin{bmatrix} {}^0_6\mathbf{R} & 0_{3 \times 3} \\ 0_{3 \times 3} & {}^0_6\mathbf{R} \end{bmatrix} \cdot {}^0\mathbf{J}_g \quad (3.12)$$

Notably,

$$\dot{\mathbf{x}} = {}^6\mathbf{J}_g \cdot \dot{\mathbf{q}}, \quad \dot{\mathbf{q}} = {}^6\mathbf{J}_g^{-1} \cdot \dot{\mathbf{x}} \quad (3.13)$$

where

$$\dot{\mathbf{x}} = \begin{bmatrix} \dot{x} \\ \dot{y} \\ \dot{z} \\ \dot{\theta}_x \\ \dot{\theta}_y \\ \dot{\theta}_z \end{bmatrix}_{\{6\}}, \quad \dot{\mathbf{q}} = \begin{bmatrix} \dot{\theta}_1 \\ \dot{\theta}_2 \\ \dot{\theta}_3 \\ \dot{\theta}_4 \\ \dot{\theta}_5 \\ \dot{\theta}_6 \end{bmatrix}$$

### Analytical Jacobian

The linear velocity of analytical Jacobian and geometric Jacobian is the same as shown in Eq 3.3. Nevertheless, as for angular velocity, analytical Jacobian takes the orientation  $(\alpha, \beta, \gamma)$  of the end effector into consideration. First of all, we investigate the relationship between the axis angle and the orientation of the end effector as following.

$$\begin{aligned} \begin{bmatrix} \theta_x \\ \theta_y \\ \theta_z \end{bmatrix} &= \begin{bmatrix} \alpha \\ 0 \\ 0 \end{bmatrix} + R_x(\alpha) \begin{bmatrix} 0 \\ \beta \\ 0 \end{bmatrix} + R_x(\alpha)R_y(\beta) \begin{bmatrix} 0 \\ 0 \\ \gamma \end{bmatrix} \\ &= \begin{bmatrix} 1 & 0 & S_\beta \\ 0 & C_\alpha & -S_\alpha C_\beta \\ 0 & S_\alpha & C_\alpha C_\beta \end{bmatrix} \begin{bmatrix} \alpha \\ \beta \\ \gamma \end{bmatrix} \end{aligned} \quad (3.14)$$



Then, utilize this generalized vector to get its Jacobian matrix  $\mathbf{J}_{\text{we}}$ .

$$\begin{bmatrix} \dot{\theta}_x \\ \dot{\theta}_y \\ \dot{\theta}_z \end{bmatrix} = \mathbf{J}_{\text{we}} \cdot \begin{bmatrix} \dot{\alpha} \\ \dot{\beta} \\ \dot{\gamma} \end{bmatrix} \quad (3.15)$$

where

$$\mathbf{J}_{\text{we}} = \begin{bmatrix} 1 & \gamma C_\beta & S_\beta \\ -\beta S_\alpha - \gamma C_\alpha C_\beta & C_\alpha + \gamma S_\alpha S_\beta & -C_\beta S_\alpha \\ \beta C_\alpha - \gamma C_\beta S_\alpha & S_\alpha - \gamma C_\alpha S_\beta & C_\alpha C_\beta \end{bmatrix} \quad (3.16)$$

Therefore,

$$\begin{bmatrix} \dot{x} \\ \dot{y} \\ \dot{z} \\ \dot{\theta}_x \\ \dot{\theta}_y \\ \dot{\theta}_z \end{bmatrix} = \begin{bmatrix} \mathbf{I}_{3 \times 3} & 0_{3 \times 3} \\ 0_{3 \times 3} & \mathbf{J}_{\text{we}} \end{bmatrix} \begin{bmatrix} \dot{x} \\ \dot{y} \\ \dot{z} \\ \dot{\alpha} \\ \dot{\beta} \\ \dot{\gamma} \end{bmatrix} \quad (3.17)$$

Finally, we obtain the relationship between geometric and analytical Jacobian.

$$\mathbf{J}_{\text{g}} = \begin{bmatrix} \mathbf{I}_{3 \times 3} & 0_{3 \times 3} \\ 0_{3 \times 3} & \mathbf{J}_{\text{we}} \end{bmatrix} \mathbf{J}_{\text{a}}, \quad \mathbf{J}_{\text{g}} = \begin{bmatrix} \mathbf{I}_{3 \times 3} & 0_{3 \times 3} \\ 0_{3 \times 3} & \mathbf{J}_{\text{we}}^{-1} \end{bmatrix} \mathbf{J}_{\text{a}} \quad (3.18)$$

### 3.4 Coordinate Transformation of the Robot Arm

So far, with the forward and inverse kinematics, the robot arm can translate and rotate around frame{6}. However, we do not see the origin of the frame{6}

as an operating point. Because the F/T sensor and a detachable end effector will be both mounted on the wrist, the tooltip position is what we want. That means we should let the robot arm know how to translate and rotate in frame $\{T\}$  instead of frame $\{6\}$ . If we have translation and rotation information of the tooltip, there is an easy way to directly give the above information to the robot arm. SetTRF  $(x,y,z,\alpha,\beta,\gamma)$  is the command of the robot arm, whose  $(x,y,z)$  is translation vector and  $(\alpha,\beta,\gamma)$  is rotation vector in representation of Euler angle .

To obtain translation and rotation vector, we respectively introduce Tool Center Point in section 3.4.1 to find the translation vector and propose an approach in section 3.4.2 to find the rotation vector.

### 3.4.1 Translation Analysis - Tool Center Point

Tool Center Point (TCP) is a critical problem for robot arm control [9]. In the previous section, we have calculated the forward and inverse kinematics of the robot arm. By Calculating kinematics, we can keep track of the origin of the frame $\{6\}$ , which is observed from the base frame. The robot arm has the capability to translate and rotate with the origin of the frame $\{6\}$ . The overhead motions are like a remote center motion (RCM). We should find the position of the tooltip and make it be an RCM point. Nevertheless, it's inefficient to recalculate the transformation matrix via mechanism dimension when changing an end effector or a tool (root canal reamer).

In order to overcome this problem, we interpret the four-points method to

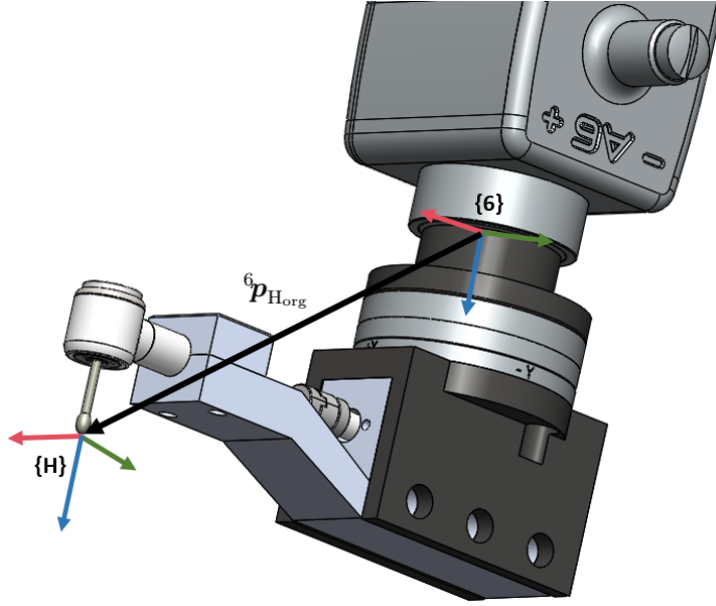


Figure 3.4: Schematic diagram for Tool Center Point. The translation vector  ${}^6p_{Horg}$  denotes the origin position relative to the frame  $\{6\}$ .

obtain the tooltip position, which is also the translation vector.

From Fig 3.2, we can obtain the following transformation matrix,

$${}^B_H\mathbf{T} = {}^B_6\mathbf{T} \cdot {}^6_H\mathbf{T} \quad (3.19)$$

and it can be rewritten as

$$\begin{aligned} \begin{bmatrix} {}^B_H\mathbf{R} & {}^Bp_{Horg} \\ 0 & 1 \end{bmatrix} &= \begin{bmatrix} {}^B_6\mathbf{R} & {}^Bp_{6org} \\ 0 & 1 \end{bmatrix} \begin{bmatrix} {}^6_H\mathbf{R} & {}^6p_{Horg} \\ 0 & 1 \end{bmatrix} \\ &= \begin{bmatrix} {}^B_6\mathbf{R} \cdot {}^6_H\mathbf{R} & {}^B_6\mathbf{R} \cdot {}^6p_{Horg} + {}^Bp_{6org} \\ 0 & 1 \end{bmatrix} \end{aligned} \quad (3.20)$$

Consequently, we get a crucial equation:

$${}^Bp_{Horg} = {}^B_6\mathbf{R} \cdot {}^6p_{Horg} + {}^Bp_{6org} \quad (3.21)$$

Now, we move the tooltip to a fixed point with four different poses, including position and orientation. Then, we will get four different rotation matrices and vectors in real-time.

$$\begin{aligned}
{}^B\mathbf{p}_{\text{Horg}} &= {}^B_F\mathbf{R}^1 \cdot {}^6\mathbf{p}_{\text{Horg}} + {}^B_F\mathbf{p}_{\text{Forg}}^1 \\
&= {}^B_F\mathbf{R}^2 \cdot {}^6\mathbf{p}_{\text{Horg}} + {}^B_F\mathbf{p}_{\text{Forg}}^2 \\
&= {}^B_F\mathbf{R}^3 \cdot {}^6\mathbf{p}_{\text{Horg}} + {}^B_F\mathbf{p}_{\text{Forg}}^3 \\
&= {}^B_F\mathbf{R}^4 \cdot {}^6\mathbf{p}_{\text{Horg}} + {}^B_F\mathbf{p}_{\text{Forg}}^4
\end{aligned} \tag{3.22}$$

In order to extract  ${}^6\mathbf{p}_{\text{Horg}}$  from Eq.3.22, we subtract the second to forth equation from the first equation.

$$\begin{bmatrix} {}^B_F\mathbf{R}^1 - {}^B_F\mathbf{R}^2 \\ {}^B_F\mathbf{R}^1 - {}^B_F\mathbf{R}^3 \\ {}^B_F\mathbf{R}^1 - {}^B_F\mathbf{R}^4 \end{bmatrix} \cdot {}^6\mathbf{p}_{\text{Horg}} = \begin{bmatrix} {}^B_F\mathbf{p}_{\text{Forg}}^2 - {}^B_F\mathbf{p}_{\text{Forg}}^1 \\ {}^B_F\mathbf{p}_{\text{Forg}}^3 - {}^B_F\mathbf{p}_{\text{Forg}}^1 \\ {}^B_F\mathbf{p}_{\text{Forg}}^4 - {}^B_F\mathbf{p}_{\text{Forg}}^1 \end{bmatrix} \tag{3.23}$$

where we define

$$\mathbf{R} = \begin{bmatrix} {}^B_F\mathbf{R}^1 - {}^B_F\mathbf{R}^2 \\ {}^B_F\mathbf{R}^1 - {}^B_F\mathbf{R}^3 \\ {}^B_F\mathbf{R}^1 - {}^B_F\mathbf{R}^4 \end{bmatrix}_{9 \times 3}, \mathbf{p} = \begin{bmatrix} {}^B_F\mathbf{p}_{\text{Forg}}^2 - {}^B_F\mathbf{p}_{\text{Forg}}^1 \\ {}^B_F\mathbf{p}_{\text{Forg}}^3 - {}^B_F\mathbf{p}_{\text{Forg}}^1 \\ {}^B_F\mathbf{p}_{\text{Forg}}^4 - {}^B_F\mathbf{p}_{\text{Forg}}^1 \end{bmatrix}_{9 \times 1}$$

Therefore,

$$\begin{aligned}
{}^6\mathbf{p}_{\text{Horg}} &= \mathbf{R}^\dagger \cdot \mathbf{p} \\
&= (\mathbf{R}^\top \mathbf{R})^{-1} \mathbf{R}^\top \cdot \mathbf{p}
\end{aligned}$$

As a result, we can utilize the four-points method to obtain the translation vector.

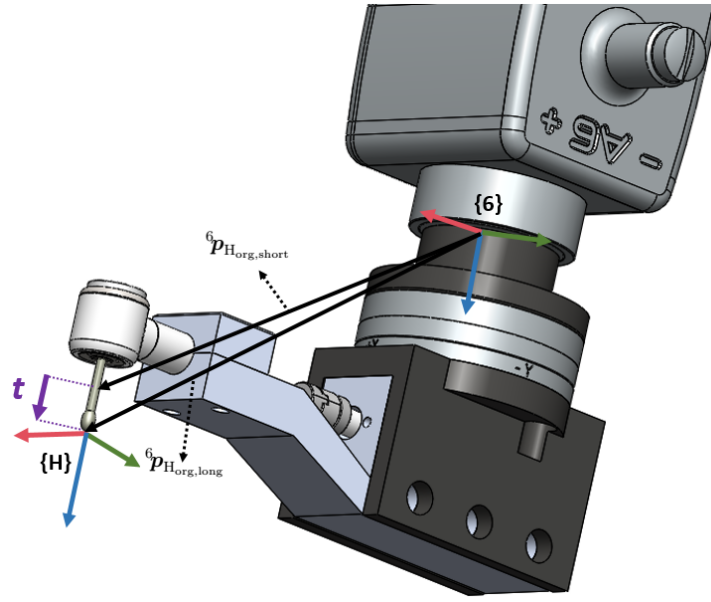


Figure 3.5: Schematic diagram for obtaining the tool vector.

### 3.4.2 Rotation Analysis

We are turning now to the discussion about the rotation vector. Above all, we have to find the vector of tool insertion direction  $t$ . We can obtain the translation vector from the origin of frame {6} to the tooltip through the TCP method. Accordingly, we use two root canal files with different lengths and apply the TCP method to separately obtain two vectors illustrated as Fig 3.4. Hence,

$$t = {}^6p_{H_{org},long} - {}^6p_{H_{org},short} \quad (3.24)$$

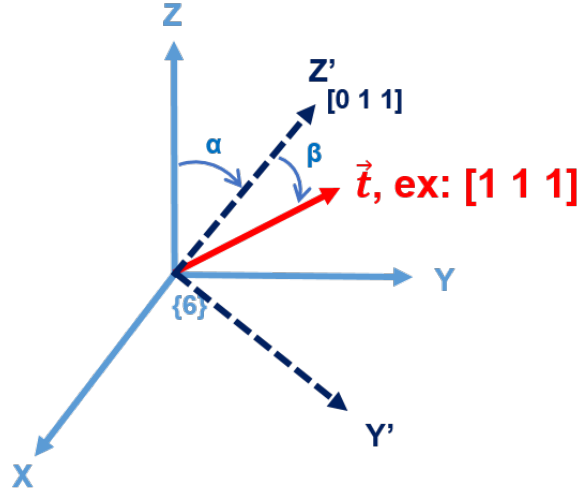


Figure 3.6: Illustration of finding the rotation matrix

For analyzing it easily, we depict it in Fig 3.5. Note that here we only discuss rotation, so we assume that we have done translation and matched the frame  $\{S\}$  with frame  $\{6\}$ . Because we hope to send a Z-axis command to achieve tool insertion, we should align the original Z-axis to the target vector. Nevertheless, Z-axis alignment without other restrictions will produce many solutions. We choose one of the solutions to align Z-axis to the target vector. According to the figure, we assume the target vector  $\mathbf{t}$  is  $[x, y, z]$ , whose projection to yz-plane  $\text{proj}_{(y-z)} \mathbf{t}$  is  $[0, y, z]$ . Initially, we rotate  $\alpha$  degree around X-axis to make original Z-axis align the projection  $[0, y, z]$ . Next, we rotate  $\beta$  degree around  $Y'$  axis and finally align the original Z-axis to the target vector  $[1,1,1]$ . The following equation

$${}^T_6 \mathbf{R} = \mathbf{R}_x(\alpha) \cdot \mathbf{R}_y(\beta) \quad (3.25)$$

where

$$\begin{aligned}\alpha &= -\text{sign}(t_y) \cdot \cos^{-1} \left( \frac{\hat{k} \cdot \text{proj}_{(y-z)} \mathbf{t}}{\|\hat{k}\| \cdot \|\text{proj}_{(y-z)} \mathbf{t}\|} \right) \\ \beta &= \text{sign}(t_x) \cdot \cos^{-1} \left( \frac{\mathbf{t} \cdot \text{proj}_{(y-z)} \mathbf{t}}{\|\mathbf{t}\| \cdot \|\text{proj}_{(y-z)} \mathbf{t}\|} \right)\end{aligned}\tag{3.26}$$

Assume  $\mathbf{t} = [x, y, z]$ ,

$$\begin{aligned}\alpha &= -\text{sign}(y) \cdot \cos^{-1} \left( \frac{z^2}{\sqrt{y^2 + z^2}} \right) \text{rad} \\ \beta &= \text{sign}(x) \cdot \cos^{-1} \left( \frac{y^2 + z^2}{\sqrt{x^2 + y^2 + z^2} \sqrt{x^2 + y^2 + z^2}} \right) \text{rad}\end{aligned}\tag{3.27}$$

$\alpha$  and  $\beta$  are Euler angles, which meet the command demand.

In this section, we have demonstrated two key aspects of reference frame changing of the robot arm. It's easy to input the results of section 3.4.1 and section 3.4.2 via the command `setTRF`, the robot arm will recognize frame{T}. Having discussed how to combine a robot arm with an end effector, the next section addresses ways of combining an F/T sensor.





# Chapter 4

## Force-Guided Robot Alignment

This chapter follows from the previous issue about integration. We continue to demonstrate some technical solutions for system integration. On top of that, the Forces and Torques (F/T) sensor will be included to discuss. Therefore, you can see the chapter as an operating manual when you simultaneously own a robot arm, an F/T sensor, and an end effector. First of all, we will explain why we need to use the F/T sensor in our project in section 4.1. Furthermore, we will introduce how to compensate the gravity affection while moving the robot in section 4.2. Admittance control based on F/T sensor will be described in section 4.3.1. Coordinate transformation of F/T sensor will be interpreted in section 4.4.1. Last but not least, we will discuss affection of setting admittance control parameters in section 4.5.

## 4.1 Problem Definition

In modern robot-assisted surgery, to simulate the eyes of doctors, image processing is often considered. With the image's information, the surgeon can obtain real-time data that humans can not observe clearly. Surgeons use the image process to do many things, such as tracking whether the patient is moving, positioning an incision point, and navigating an insertion path. As for root canal treatment, the endodontist checks the number of root canals with computed tomography. Before starting to clean the pulp, the endodontist tries to insert root files into root canals. Then the endodontist takes the patient to have computed tomography(CT). CT scan can clearly show the tooth with the root files. With the preoperative image, the endodontist can check whether all root canals are all found and determine all root canals' lengths. However, the above image application is preoperative. The endodontist can only use the preoperative image to guess the direction of the insertion. The intraoperative image processing is absent due to the dimension restriction of a tooth. It is difficult to get a real-time image when the dentist inserts a root file into the opened tooth because it will obstacle the observation. Besides, the diameter of a root canal is 1 mm and is smaller than a root file. It is impossible to get the image from any shooting angle.

To solve the first problem - without image processing, we propose a method based on force-guided. We surveyed the peg-in-hole based on F/T sensor feedback [10] because the cleaning procedure is similar to it. On the other hand, we provide two operating modes - "Dragging Mode" and "Self-Alignment Mode" to cooperate

with a dentist. In "Dragging Mode", we can hold the handpiece to the desired position and orientation. We hope to use this mode to let the dentist move the handpiece to the injured tooth. In "Self-Alignment Mode", the handpiece can automatically align the root canal direction even though there are many complicated conditions with different teeth.

## 4.2 Integration of F/T sensor

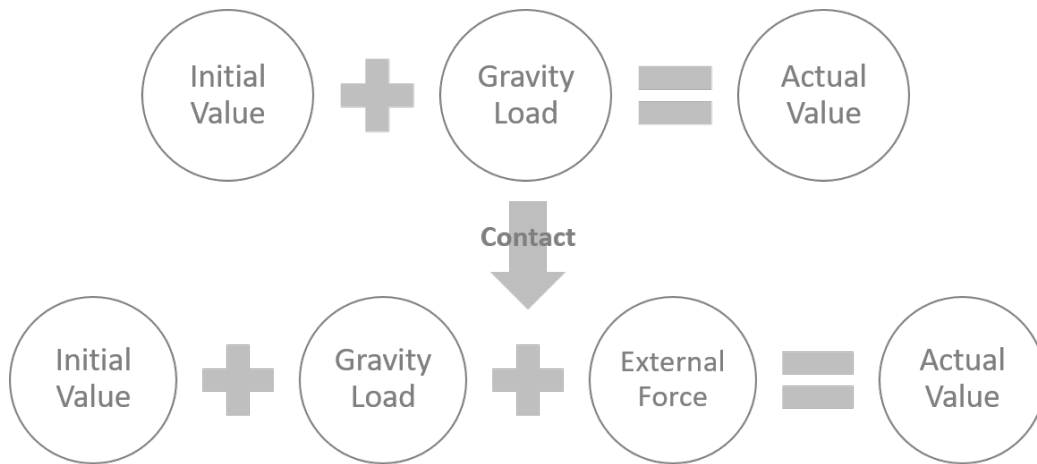


Figure 4.1: Data Analysis of F/T sensor.

Gravity compensation is a critical technical issue when combining an F/T sensor with a robot arm and an end effector [11]. Fundamentally, we should receive stable data when a static F/T sensor bears the same load or force. Nevertheless, our F/T sensor is installed on the robot arm and move with the pose of the robot arm. On account of its mobility, the gravity of the end effector will significantly affect

the actual value we received. Moreover, starting without resetting the F/T sensor to zero would lead to an initial value. If we could not analyze the actual value to an initial value and a gravity load, we would obtain an unstable actual value, not to mention the external force caused by contact force.

Therefore, we illustrate a method, which is to analyze the actual value of the F/T sensor to an initial value and gravity load in real-time. It's worth noting that with this approach, we can get the installation angle between the F/T sensor and the robot arm, including assembly error, and we no longer need to reset the F/T sensor to zero every time.

### The Centroid Position of End Effector

To start with the first equation in Figure 4.1,

Initial value + Gravity Load = Actual Value

$$\Rightarrow \begin{cases} \mathbf{f}_0 + \mathbf{f}_g = \mathbf{f} \\ \boldsymbol{\tau}_0 + \boldsymbol{\tau}_g = \boldsymbol{\tau} \end{cases} \Rightarrow \begin{cases} f_{0x} + f_{gx} = f_x \\ f_{0y} + f_{gy} = f_y \\ f_{0z} + f_{gz} = f_z \\ \tau_{0x} + \tau_{gx} = \tau_x \\ \tau_{0y} + \tau_{gy} = \tau_y \\ \tau_{0z} + \tau_{gz} = \tau_z \end{cases} \quad (4.1)$$

where  $\mathbf{f}$  and  $\boldsymbol{\tau}$  are force and torque vector respectively.

And, by terms of moment arm formula,

$$\because \boldsymbol{\tau}_g = \mathbf{r} \times \mathbf{f}_g \quad (4.2)$$

where  $\mathbf{r}$  denotes the centroid position of the end effector in the sensor frame.

$$\begin{aligned}\therefore \boldsymbol{\tau} &= \boldsymbol{\tau}_0 + \boldsymbol{\tau}_g \\ &= \boldsymbol{\tau}_0 + \mathbf{r} \times \mathbf{f}_g\end{aligned}\tag{4.3}$$

Then, Substitute the first line of Equation 4.1 into the above equation, we will obtain

$$\boldsymbol{\tau} = \boldsymbol{\tau}_0 + \mathbf{p} \times (\mathbf{f} - \mathbf{f}_0)\tag{4.4}$$

, which could be extended as

$$\begin{cases} \tau_x = \tau_{0x} + (f_z - f_{0z}) \cdot y - (f_y - f_{0y}) \cdot z \\ \tau_y = \tau_{0y} + (f_x - f_{0x}) \cdot z - (f_z - f_{0z}) \cdot x \\ \tau_z = \tau_{0z} + (f_y - f_{0y}) \cdot x - (f_x - f_{0x}) \cdot y \end{cases}\tag{4.5}$$

and be overwritten as

$$\begin{bmatrix} \tau_x \\ \tau_y \\ \tau_z \end{bmatrix} = \begin{bmatrix} 0 & f_z & -f_y & 1 & 0 & 0 \\ -f_z & 0 & f_x & 0 & 1 & 0 \\ f_y & -f_x & 0 & 0 & 0 & 1 \end{bmatrix} \begin{bmatrix} x \\ y \\ z \\ k_1 \\ k_2 \\ k_3 \end{bmatrix}\tag{4.6}$$

where

$$\begin{cases} k_1 = \tau_{0x} - (f_{0z} \cdot y + f_{0y} \cdot z) \\ k_2 = \tau_{0y} - (f_{0x} \cdot z + f_{0z} \cdot x) \\ k_3 = \tau_{0z} - (f_{0y} \cdot x + f_{0x} \cdot y) \end{cases} \text{ are all constant}\tag{4.7}$$

With extracting  $[x, y, z, k_1, k_2, k_3]$  in mind, we move the robot arm to  $n$  ( $n \geq 3$ ) positions with different poses. By recording  $n$  torque vectors and corresponding  $n$  force vectors from F/T sensor, we can expand Equation 4.6 as

$$\begin{bmatrix} \tau_x^1 \\ \tau_y^1 \\ \tau_z^1 \\ \tau_x^2 \\ \tau_y^2 \\ \tau_z^2 \\ \vdots \\ \tau_x^n \\ \tau_y^n \\ \tau_z^n \end{bmatrix} = \begin{bmatrix} 0 & f_z^1 & -f_y^1 & 1 & 0 & 0 \\ -f_z^1 & 0 & f_x^1 & 0 & 1 & 0 \\ f_y^1 & -f_x^1 & 0 & 0 & 0 & 1 \\ 0 & f_z^2 & -f_y^2 & 1 & 0 & 0 \\ -f_z^2 & 0 & f_x^2 & 0 & 1 & 0 \\ f_y^2 & -f_x^2 & 0 & 0 & 0 & 1 \\ \vdots & & \vdots & & & \\ 0 & f_z^3 & -f_y^3 & 1 & 0 & 0 \\ -f_z^3 & 0 & f_x^3 & 0 & 1 & 0 \\ f_y^3 & -f_x^3 & 0 & 0 & 0 & 1 \end{bmatrix} \begin{bmatrix} x \\ y \\ z \\ k_1 \\ k_2 \\ k_3 \end{bmatrix} \quad (4.8)$$

, which is defined as

$$\mathbf{m}_{(3n \times 1)} = \mathbf{F}_{(3n \times 6)} \cdot \mathbf{p}_{(6 \times 1)} \quad (4.9)$$

As a consequence of the full column rank of  $\mathbf{F}$ , we can apply Moore-Penrose pseudoinverse. Then,

$$\begin{aligned} \mathbf{p} &= \mathbf{F}^\dagger \cdot \mathbf{m} \\ &= (\mathbf{F}^\top \mathbf{F})^{-1} \mathbf{F}^\top \cdot \mathbf{m} \end{aligned}$$

From now on, we have already known the centroid position of end effector in the sensor frame and values of the constants  $k_1, k_2, k_3$ .

### Gravity Compensation and Initial Value Reset

Next, let us return to the first equation in Figure 4.1. We continue to use this formula and contemplate it from the perspective of coordinate transformation relation. Here we hypothesize that the end effector weighs  $g$  kilograms relative to the frame  $\{0\}$  which is also the world frame. That means the gravity vector of the end effector  ${}^0\mathbf{g}$  is  $[0, 0, -g]$  in the frame  $\{0\}$ . Then, we can derive it as following.

$$\text{Initial value} + \text{Gravity Load} = \text{Actual Value} \quad (4.10)$$

$$\Rightarrow \mathbf{f}_0 + {}^S_6\mathbf{R} \cdot {}^6_0\mathbf{R} \cdot {}^0\mathbf{g} = \mathbf{f}$$

which is relative to frame  $\{6\}$ . Hence, we assume an installation angle  $\theta$  including assembly error.

$${}^S_6\mathbf{R} = \begin{bmatrix} \cos(\theta) & \sin(\theta) & 0 \\ -\sin(\theta) & \cos(\theta) & 0 \\ 0 & 0 & 1 \end{bmatrix} \quad (4.11)$$

Besides, we can easily calculate  ${}^6_0\mathbf{R}$  from Equation 3.3.2.

$$\begin{aligned} {}^6_0\mathbf{R} &= {}^0_6\mathbf{R}^\top \\ &:= \begin{bmatrix} r_{11} & r_{12} & r_{13} \\ r_{21} & r_{22} & r_{23} \\ r_{31} & r_{32} & r_{33} \end{bmatrix} \end{aligned} \quad (4.12)$$

Therefore,

$$\begin{bmatrix} f_{0x} \\ f_{0y} \\ f_{0z} \end{bmatrix} + \begin{bmatrix} \cos(\theta) & \sin(\theta) & 0 \\ -\sin(\theta) & \cos(\theta) & 0 \\ 0 & 0 & 1 \end{bmatrix} \begin{bmatrix} r_{11} & r_{12} & r_{13} \\ r_{21} & r_{22} & r_{23} \\ r_{31} & r_{32} & r_{33} \end{bmatrix} \begin{bmatrix} 0 \\ 0 \\ -g \end{bmatrix} = \begin{bmatrix} f_x \\ f_y \\ f_z \end{bmatrix} \quad (4.13)$$

Further, we rewrite it as

$$\begin{bmatrix} -r_{13} & -r_{23} & 0 & 1 & 0 & 0 \\ -r_{23} & r_{13} & 0 & 0 & 1 & 0 \\ 0 & 0 & -r_{33} & 0 & 0 & 1 \end{bmatrix} \begin{bmatrix} g \cos(\theta) \\ g \sin(\theta) \\ g \\ f_{0x} \\ f_{0y} \\ f_{0z} \end{bmatrix} = \begin{bmatrix} f_x \\ f_y \\ f_z \end{bmatrix} \quad (4.14)$$

In the same way as Equation 4.6, we can extract  $[g \cos(\theta), g \sin(\theta), g, f_{0x}, f_{0y}, f_{0z}]$  by the least square solution. Note that, we can simultaneously record these data when using the method in Equation 4.6. By recording  $n(n \geq 3)$  third columns of rotation matrices and corresponding  $n$  force vectors from F/T sensor, we can expand Equation 4.14 as

$$\begin{bmatrix} -r_{13}^1 & -r_{23}^1 & 0 & 1 & 0 & 0 \\ -r_{23}^1 & r_{13}^1 & 0 & 0 & 1 & 0 \\ 0 & 0 & -r_{33}^1 & 0 & 0 & 1 \\ -r_{13}^2 & -r_{23}^2 & 0 & 1 & 0 & 0 \\ -r_{23}^2 & r_{13}^2 & 0 & 0 & 1 & 0 \\ 0 & 0 & -r_{33}^2 & 0 & 0 & 1 \\ \vdots & & & & & \\ -r_{13}^n & -r_{23}^n & 0 & 1 & 0 & 0 \\ -r_{23}^n & r_{13}^n & 0 & 0 & 1 & 0 \\ 0 & 0 & -r_{33}^n & 0 & 0 & 1 \end{bmatrix} \begin{bmatrix} g \cos(\theta) \\ g \sin(\theta) \\ g \\ f_{0x} \\ f_{0y} \\ f_{0z} \end{bmatrix} = \begin{bmatrix} f_{0x}^1 \\ f_{0y}^1 \\ f_{0z}^1 \\ f_{0x}^2 \\ f_{0y}^2 \\ f_{0z}^2 \\ \vdots \\ f_{0x}^n \\ f_{0y}^n \\ f_{0z}^n \end{bmatrix} \quad (4.15)$$



, which is defined as

$$\mathbf{M}_{(3n \times 6)} \cdot \mathbf{p}_{(6 \times 1)} = \mathbf{f}_{(3n \times 1)} \quad (4.16)$$

As a consequence of the full column rank of  $\mathbf{M}$ , we can apply Moore-Penrose pseudoinverse. Then,

$$\begin{aligned} \mathbf{p} &= \mathbf{M}^\dagger \cdot \mathbf{f} \\ &= (\mathbf{M}^\top \mathbf{M})^{-1} \mathbf{M}^\top \cdot \mathbf{f} \end{aligned}$$

Apparently, we can directly obtain  $g, f_{0x}, f_{0y}, f_{0z}$ . Afterwards, we substitute them into Equation 4.7 to calculate

$$\begin{cases} \tau_{0x} = k_1 + (f_{0z} \cdot y + f_{0y} \cdot z) \\ \tau_{0y} = k_2 + (f_{0x} \cdot z + f_{0z} \cdot x) \\ \tau_{0z} = k_3 + (f_{0y} \cdot x + f_{0x} \cdot y) \end{cases} \quad (4.17)$$

Finally, we successfully obtain the weight of the end effector  $g$ , the initial value of the F/T sensor  $[f_{0x}, f_{0y}, f_{0z}, \tau_{0x}, \tau_{0y}, \tau_{0z}]$ .

As for installation angle  $\theta$  including assembly error, there is an further discussion. Undoubtedly, we can derive it as

$$\theta = \cos^{-1} \left( \frac{g \cos(\theta)}{g} \right) \text{ or } \sin^{-1} \left( \frac{g \sin(\theta)}{g} \right) \quad (4.18)$$

In theory, By either the arccos function or arcsin function, we can derive the same value. However, we estimate  $[g \cos(\theta), g \sin(\theta), g, f_{0x}, f_{0y}, f_{0z}]$  by using the least square solution which produce a approximated answer rather than the correct answer. A subtle bias caused by the least square solution will be enlarged through

the arc function. Thankfully, we originally designed an adapter to connect the robot arm and F/T sensor, and the installation angle is exactly zero degrees. Therefore, here we only need to concern about the subtle bias result from assembly errors.

Here we take the same bias and compare arccos to arcsin. Obviously, if we

Table 4.1: Arc-function Comparison

bias $n$ (rad)	$\sin^{-1}(n)$ (degree)	$\cos^{-1}(1 - n)$ (degree)
0	0	0
0.001	0.057	2.56
0.01	0.57	8.11
0.1	5.7	25.84

separately give the same bias ( 0.1 rad) into the arccos and arcsin function, the arccos function will enlarge the bias significantly larger than the arcsin function.

Hence we should use

$$\theta = \sin^{-1} \left( \frac{g \sin(\theta)}{g} \right) \quad (4.19)$$

Notably, as a result of the zero installation angle we initially designed from Table 4.1, we could infer using the arcsin function. In contrast, if the installation angle is not zero, the above assumption will be invalid.

Ultimately, we have successfully dissected the actual value of the F/T sensor into the initial value of the F/T sensor and the gravity of the end effector.

### External Force Evaluation

Next, we continue to review the second equation in Figure 4.1.

Initial value + Gravity Load + External Force = Actual Value

$$\Rightarrow \begin{cases} \mathbf{f}_0 + \mathbf{f}_g + \mathbf{f}_e = \mathbf{f} \\ \boldsymbol{\tau}_0 + \boldsymbol{\tau}_g + \boldsymbol{\tau}_e = \boldsymbol{\tau} \end{cases} \quad (4.20)$$

Therefore,

$$\begin{aligned} \mathbf{f}_e &= \mathbf{f} - \mathbf{f}_0 - \mathbf{f}_g \\ &= \mathbf{f} - \mathbf{f}_0 - {}^S_6\mathbf{R} \cdot {}^0_6\mathbf{R} \cdot \mathbf{g} \\ \boldsymbol{\tau}_e &= \boldsymbol{\tau} - \boldsymbol{\tau}_0 - \boldsymbol{\tau}_g \\ &= \boldsymbol{\tau} - \boldsymbol{\tau}_0 - \mathbf{r} \times \mathbf{f}_g \end{aligned} \quad (4.21)$$

$$\Rightarrow \begin{cases} f_{ex} = f_x - f_{0x} + g \cos(\theta)r_{13} + g \sin(\theta)r_{23} \\ f_{ey} = f_y - f_{0y} - g \sin(\theta)r_{13} + g \cos(\theta)r_{23} \\ f_{ez} = f_z - f_{0z} + gr_{33} \\ \tau_{ex} = f_x - \tau_{0x} - (g_z \cdot y - g_y \cdot z) \\ \tau_{ey} = f_y - \tau_{0y} - (g_x \cdot z - g_z \cdot x) \\ \tau_{ez} = f_z - \tau_{0z} - (g_y \cdot x - g_x \cdot y) \end{cases}$$

## 4.3 Dragging Mode

In the hope that dentist could drag our system to an infected tooth by holding the end effector, we usher in admittance control based on F/T sensor.

### 4.3.1 Admittance Control based on F/T sensor

#### Control Scheme

Admittance control makes the robot move like a spring-mass-damper system. Forces and torques can be mapped into the movements such as position or velocity. Most importantly, admittance control enables a robot arm to cooperate with humans in a safe work environment. Since Meca500 is an industrial robot arm without admittance control, we subsequently combine the robot arm with the F/T sensor to adopt admittance control. With force and torque feedback, the F/T sensor makes Meca500 be like a collaborative robot arm. Therefore, we propose a control scheme depicted as Figure 4.2. It's worth noting that in this approach, the admittance control function is triggered by the end effector mounted on the F/T sensor instead of detecting each wrist torque of the robot arm.

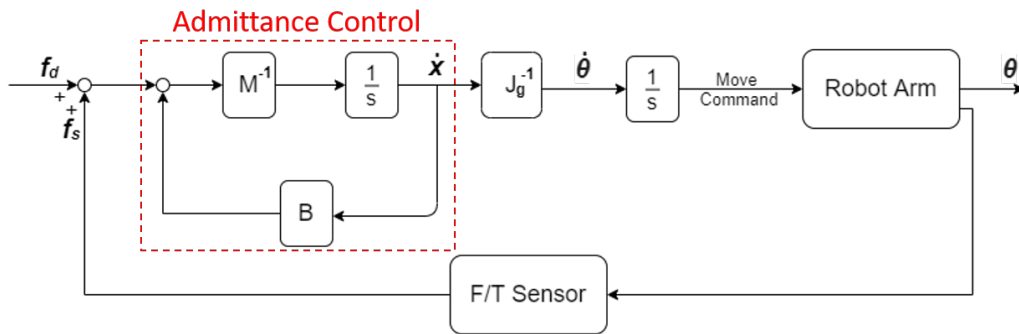


Figure 4.2: Control scheme.  $f_d$  denotes the desired forces and torques vector.  $f_s$  denotes the real value detected by F/T sensor and is also a forces and torques vector.  $\dot{x}$  denotes  $[\dot{x}, \dot{y}, \dot{z}, \dot{\theta}_x, \dot{\theta}_y, \dot{\theta}_z]$ .  $J_g$  denotes the geometric Jacobian matrix.  $\dot{q}$  denotes  $[\dot{\theta}_1, \dot{\theta}_2, \dot{\theta}_3, \dot{\theta}_4, \dot{\theta}_5, \dot{\theta}_6]$ .  $q$  denotes  $[\theta_1, \theta_2, \theta_3, \theta_4, \theta_5, \theta_6]$ .

A standard equation of admittance control is represented as Equation 4.22.

The values we obtain from the F/T sensor are  $[f_x, f_y, f_z, \tau_x, \tau_y, \tau_z]$ , whose forces  $[f_x, f_y, f_z]$  are related to the translations  $[x, y, z]$  and torques  $[\tau_x, \tau_y, \tau_z]$  are related to the axis angle  $[\theta_x, \theta_y, \theta_z]$ .

$$\begin{bmatrix} x \\ y \\ z \\ \theta_x \\ \theta_y \\ \theta_z \end{bmatrix} = \frac{1}{\mathbf{M}s^2 + \mathbf{B}s + \mathbf{K}} \begin{bmatrix} f_x \\ f_y \\ f_z \\ \tau_x \\ \tau_y \\ \tau_z \end{bmatrix} \quad (4.22)$$

### Selection of Admittance Control Model

In our proposed approach, we omit parameter  $\mathbf{K}$  which is relevant to spring stiffness, considering that it's not necessary to bounce such as a spring. Therefore, our system should behave like a mass-damper system as following.

$$\begin{bmatrix} x \\ y \\ z \\ \theta_x \\ \theta_y \\ \theta_z \end{bmatrix} = \frac{1}{\mathbf{M}s^2 + \mathbf{B}s} \begin{bmatrix} f_x \\ f_y \\ f_z \\ \tau_x \\ \tau_y \\ \tau_z \end{bmatrix} \quad (4.23)$$

where  $\mathbf{M}$ ,  $\mathbf{B}$ ,  $\mathbf{K}$  are diagonal positive definite matrices. Affections of these parameters will be discussed in section 4.5.

### Robot Command Decision

After determining our admittance control model, we should select a correspondent command to move the robot. However, there are many commands of moving the robot arm, as shown in Table 4.2.

Table 4.2: Moving commands in Meca500

Types	Commands	Input parameters
Position	MoveJoints	$\theta_1, \theta_2, \theta_3, \theta_4, \theta_5, \theta_6$
	MovePose	$x, y, z, \alpha, \beta, \gamma$
Velocity	MoveJointsVel	$\dot{\theta}_1, \dot{\theta}_2, \dot{\theta}_3, \dot{\theta}_4, \dot{\theta}_5, \dot{\theta}_6$
	MoveLinVelTRF	$\dot{x}, \dot{y}, \dot{z}, \dot{\theta}_x, \dot{\theta}_y, \dot{\theta}_z$

Considering that the singularity problem is an imperative subject in robotics, we intend to use MoveJoints or MoveJointsVel to set the axes' angles directly. Despite that it's easier to implement admittance control via other commands, the system would touch the singularity point at any time. It undoubtedly exposes patients to danger because of the uncertainty of the system. In our case, we could detect whether it is a singularity or not before commanding the robot. Therefore, position command - MoveJoints and velocity command - MoveJointsVel is our option. Why we choose the command MoveJoints is that Meca500 has a default time-out value to ensure its safety. Even though we could set this value from 0.001 to 2 seconds, Meca500 is still restricted to move with this value. For example, the value of time-out is set 0.1 sec. While the robot receives a command, the

robot move for 0.1 sec then immediately stops. It's not easy to control via velocity command due to this default property.

Finally, we designate  $\text{MoveJointsVel}(\dot{\theta}_1, \dot{\theta}_2, \dots, \dot{\theta}_6)$  as our main command. Thanks to the property of Jacobian matrix shown in Equation 3.13, we can transform  $\dot{\mathbf{x}}$  into  $\dot{\mathbf{q}}$ . Then we multiply it an integrator  $\frac{1}{s}$  to obtain  $\mathbf{q}$ . Note that, As F/T sensor is mounted on the frame{6}, we should use Equation 3.13 rather than Equation 3.6.

### Implementation in Discrete Time

To implement it in practice, we use the bilinear transformation, also known as Tustin method, to control it in discrete time.

$$\begin{aligned} \frac{\mathbf{v}(s)}{\mathbf{f}(s)} &= (\mathbf{M}s + \mathbf{B})^{-1} \\ \Rightarrow \frac{\mathbf{v}(z)}{\mathbf{f}(z)} &= \frac{T(1 + z^{-1})}{(T \cdot \mathbf{B} + 2\mathbf{M}) + (T\mathbf{B} - 2\mathbf{M}) \cdot z^{-1}} \end{aligned} \quad (4.24)$$

and,

$$\begin{aligned} \frac{\boldsymbol{\theta}(s)}{\mathbf{w}(s)} &= \frac{\mathbf{K}}{s} \\ \Rightarrow \frac{\boldsymbol{\theta}(z)}{\mathbf{w}(z)} &= \frac{T\mathbf{K}}{2} \frac{1 + z^{-1}}{1 - z^{-1}} \end{aligned} \quad (4.25)$$

Therefore,

$$\begin{aligned} \mathbf{v}[k+1] &= \frac{T}{T\mathbf{B} + 2\mathbf{M}} \cdot (\mathbf{f}[k+1] + \mathbf{f}[k]) - \frac{T\mathbf{B} - 2\mathbf{M}}{T\mathbf{B} + 2\mathbf{M}} \cdot \mathbf{v}[k] \\ \boldsymbol{\theta}[k+1] &= \boldsymbol{\theta}[k] + \frac{T\mathbf{K}}{2} (\mathbf{w}[k+1] + \mathbf{w}[k]) \end{aligned} \quad (4.26)$$

where  $T$  is the sampling time.

## 4.4 Self-Alignment Mode

This section aims to develop a framework for robot self-alignment regarding the position and orientation of the root canal, which is one of the main contributions of the thesis. This function assists endodontists in operating the cleaning procedure automatically and ensures a postoperative recovery for patients. The main idea is to amend the direction of insertion by itself to lower the contact resistance.

We propose a complete robotic procedure. First and foremost, the prominent role of this procedure is the root canal reamer. We rotate the root canal reamer to clean a pulp, move it to do reciprocation and self-alignment. So, we care about the root canal, such as its position, orientation, rotation speed, and contact force. Nevertheless, the robot arm and the F/T sensor have their coordinates initially. They originally recognize its own coordinates rather than the root canal reamer's frame, so they do their work respectively. Therefore, we need to let them understand the tool frame. Thanks to section 3.4, we have demonstrated how to change the reference frame of the robot arm. After that, we can identify the translation and rotation information of the root canal reamer and subsequently obtain the transformation matrix from the robot arm to the tool. As for the F/T sensor, we have explained how to do gravity compensation in section 4.2, we will interpret how to change its fiducial to the tooltip in section 4.4.1. Besides, we will advance motion planning in accordance with the dentist's motion and standard surgical solution in section 4.4.2



#### 4.4.1 Coordinate Transformation of F/T sensor

Similar to Coordinate transformation of F/T sensor in section 3.4. The F/T sensor originally recognizes its coordinate rather than the root canal reamer's frame. Namely, the F/T sensor receives unmatched data when the tool contacts an obstacle due to the wrong reference frame. Hence, here we illustrate how to obtain the coordinate transformation of the F/T sensor to decouple the force and torque from frame  $\{S\}$  to the frame  $\{T\}$ . We analyze it from two perspectives - reference frame changing and measurement point changing.

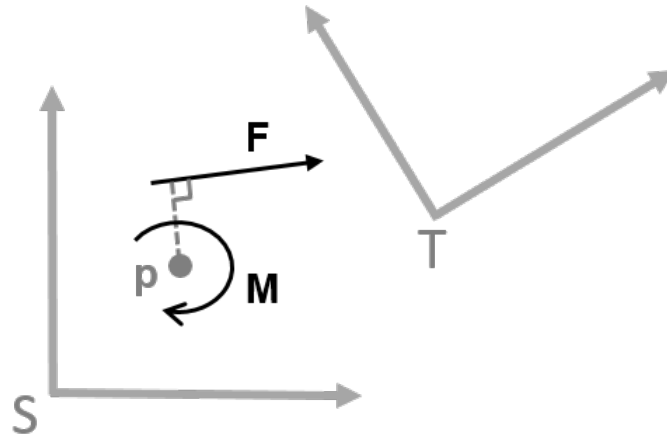


Figure 4.3: Illustration of changing reference frame from  $\{S\}$  to  $\{T\}$ .  $f$  and  $m$  respectively denote a force and a moment measured at point  $p$ .

In view of reference frame changing in Figure 4.3, we can derive the following

equation.

$$\begin{bmatrix} \mathbf{f}_p \\ \mathbf{m}_p \end{bmatrix}_{\{T\}} = \begin{bmatrix} {}^T_S \mathbf{R} & \mathbf{0} \\ \mathbf{0} & {}^T_S \mathbf{R} \end{bmatrix} \begin{bmatrix} \mathbf{f}_p \\ \mathbf{m}_p \end{bmatrix}_{\{S\}} \quad (4.27)$$

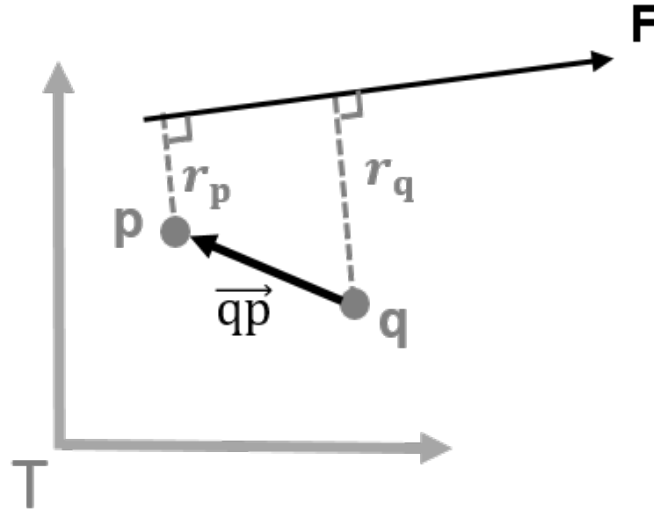


Figure 4.4: Illustration of changing reference frame from  $\{S\}$  to  $\{T\}$ .  $\mathbf{f}$  and  $\mathbf{m}$  respectively denote a force and a moment measured at point p.

On the other hand, in Figure 4.4 we describe a force and a torque observed in the same frame but at a different point.

$$\begin{aligned} \mathbf{f} &= \mathbf{f}_p = \mathbf{f}_q \\ \mathbf{m}_q &= \mathbf{r}_q \cdot \mathbf{f} \\ &= \mathbf{r}_p \cdot \mathbf{f} + \vec{qp} \times \mathbf{f}_p \\ &= \mathbf{m}_p + \vec{qp} \times \mathbf{f}_p \end{aligned} \quad (4.28)$$

Assume

$$\vec{qp} = \begin{bmatrix} u_1 \\ u_2 \\ u_3 \end{bmatrix}$$

then

$$\vec{qp} \times \mathbf{f}_p = \begin{bmatrix} 0 & -u_3 & u_2 \\ u_3 & 0 & -u_1 \\ -u_2 & u_1 & 0 \end{bmatrix} \begin{bmatrix} f_1 \\ f_2 \\ f_3 \end{bmatrix} \quad (4.29)$$

As a result, we consider reference frame changing and measurement point changing, and then we can obtain the following essential equation.

$$\begin{bmatrix} \mathbf{f}_q \\ \mathbf{m}_q \end{bmatrix}_{\{T\}} = \begin{bmatrix} \mathbf{I}_{3 \times 3} & \mathbf{0} \\ 0 & -u_3 & u_2 \\ u_3 & 0 & -u_1 \\ -u_2 & u_1 & 0 \end{bmatrix} \begin{bmatrix} {}^T_S \mathbf{R} & \mathbf{0} \\ \mathbf{0} & {}^T_S \mathbf{R} \end{bmatrix} \begin{bmatrix} \mathbf{f}_p \\ \mathbf{m}_p \end{bmatrix}_{\{S\}} \quad (4.30)$$

#### 4.4.2 Motion Planning: Based on Admittance Control

Finally, we plan a series of motions to simulate the cleaning procedure of the root canal treatment. Endodontist uses their professional experience to determine how many force to apply and when to reverse the file to release the torque caused by the contact force. Because the root canal resembles a cone, the profundity of the file is larger, the resultant force composed of contact forces is more significant. Namely, the endodontist will apply more and more pressure in the insertion direction during the surgery. To simulate this series of motions, we could directly command the

robot arm to move with the series of actions. However, commanding the robot arm is a dilemma because we have already use admittance control which also commands the robot arm to move. Therefore, to solve the conflict, we continue to utilize admittance control and propose a method based on admittance control to simulate the series of motions shown in Fig 4.5.

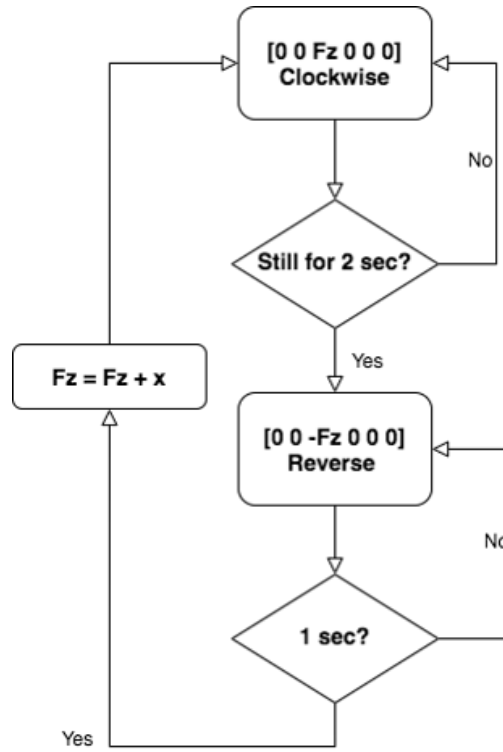


Figure 4.5: Flow chart of motion planning

## 4.5 Affections of Parameters Setting

Because our system is similar to a mass- damper system, we focus on the performance of the velocity  $\dot{x}$  whereby the system could be considered as

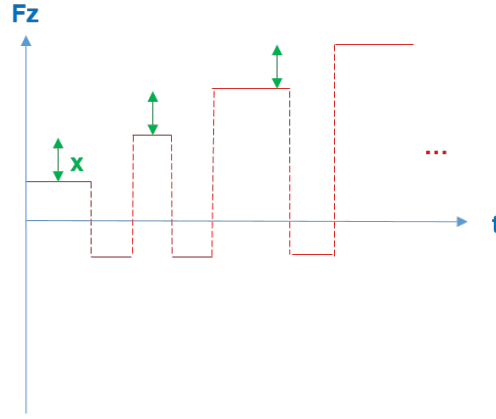


Figure 4.6: Flow chart of motion planning

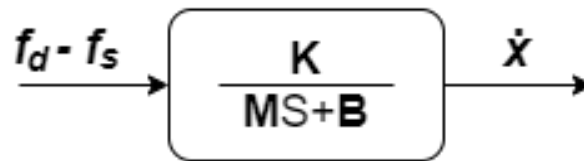


Figure 4.7: Control scheme.  $\mathbf{M}$ ,  $\mathbf{B}$ ,  $\mathbf{K}$  are all diagonal positive definite matrices, whose diagonal indexes are respectively related to  $x, y, z, \theta_x, \theta_y, \theta_z$ .  $\mathbf{M}$ ,  $\mathbf{B}$  are related to the inertial and damping respectively, and  $\mathbf{K}$  is a proportional gain.

It is a first-order control system and its step response is

$$\begin{aligned}\mathcal{L}^{-1}\left[\frac{1}{s} \cdot \frac{K}{Ms + B}\right] &= \mathcal{L}^{-1}\left[\frac{K}{B} \left(\frac{1}{s} - \frac{1}{s + \frac{B}{M}}\right)\right] \\ &= \frac{K}{B} \left(1 - e^{-\frac{B}{M}t}\right)\end{aligned}\quad (4.31)$$

From the above derivation, we can know

$$\begin{aligned}\text{time constant } \tau &= \frac{M}{B} \\ \text{gain} &= \frac{K}{B}\end{aligned}\quad (4.32)$$

Hence, the transient response can be derived as

$$\begin{aligned}\text{Rise time} &= 2.3\tau = \frac{2.3M}{B} \\ \text{Settling time} &= 4\tau = \frac{4M}{B}\end{aligned}\quad (4.33)$$

In theory, when  $\tau$  is larger, the pole is farther from the origin in  $S$  domain, the system is more stable. Besides, when  $\tau$  is larger, the response speed is faster. Furthermore, when the gain  $\frac{K}{B}$  is larger, the robot arm moves more. Therefore, we coarse-tune parameter  $K$  to adjust the whole gain of the system and determine the mode of the system is "Dragging Mode" or "Self-Alignment Mode". Last but not least, we fine-tune diagonal parameters of  $B$  separately because the inertial and spring properties of each axis are discrepant.

In practice, we implement it in discrete time. From Equation 4.24, we can further derive the final value in discrete time shown as

$$\text{gain} = \lim_{z \rightarrow 1} (z - 1) \cdot \frac{TK(z + 1)}{(TB + 2M)z + TB - 2M} \cdot \frac{1}{\frac{2}{T} \frac{z-1}{z+1}} = \frac{KT}{B} \quad (4.34)$$

Compared to the gain in continuous time, the sampling time in discrete time also effect the gain. Because the sampling time we set is 0.002s, we set  $(m_i : b_i = 1 :$

500) to make ( $\tau_i = \frac{m_i}{b_i} = 0.002$ ), then the system will rise up to 98% after 0.004 second. Further, we can alter  $\mathbf{K}$  to easily regulate the gain. In Table 4.3, we show detailed parameters with "Dragging Mode" and "Self-Alignment Mode".

Table 4.3: Parameters setting of Admittance control.

Parameter	Dragging Mode	Self-Alignment Mode
$k$	200000	100000
$b_1$	1.2	0.7
$b_2$	0.6	0.7
$b_3$	1.1	0.7
$b_4$	1.7	2
$b_5$	4	2
$b_6$	1.8	2
$\mathbf{K} = \text{diag}(k, k, k, k, k, k), \quad \mathbf{B} = \text{diag}(b_1, b_2, b_3, b_4, b_5, b_6)$		

In "Dragging Mode", we hold the handpiece to move as shown in Fig 4.8. Due to different level arms, the forces we apply in each axis are all different. Therefore, to provide users a good experience, we set each parameter of  $\mathbf{B}$  of "Dragging mode" with different values. With these different values, the users can comfortably move the robot arm to the desired position and orientation. On the other hand, in "Self-Alignment Mode", an external force is applied at the tool, and we have already transformed the reference frame of the F/T sensor. We set the first three variables relative to the linear velocity as the same values. Besides, We set the last

three variables relative to the angular velocity as the other same values.

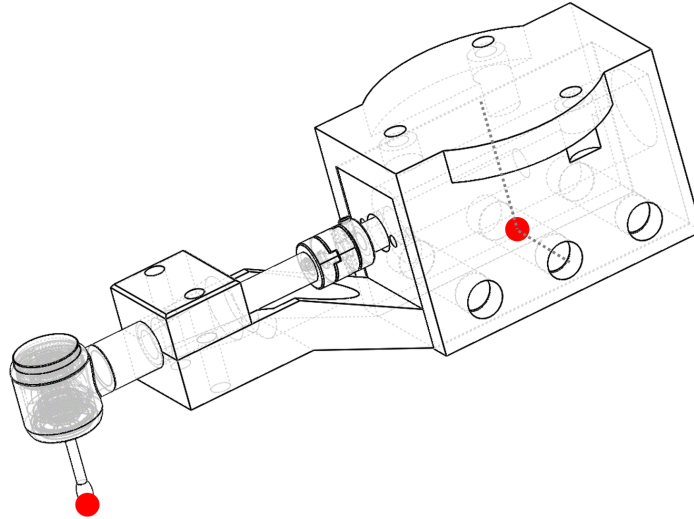


Figure 4.8: Holding gesture in "Dragging Mode"



# **Chapter 5**

## **Control of Endodontic File Rotation**

### **5.1 Problem Definition**

(Main cause of Files Fracture instrument fracture)

(File property)

### **5.2 The Proposed Method and Theorem**

(CACS2020 Prototype 1)

(Motion Planning: sections)(Current threshold setting)

Once the current of the file is in excess of the threshold, it will inversely rotate to release torque. A decline(decrease/increase/drop) in the current of the motor is indicative of contact resistance of the file.



# Chapter 6

## Preliminary Experiment Result

### 6.1 Experimental Setup

Use present tense.

(Communication protocol – EtherCAT, RTOS – NI target)

For 6.2 experiment: (Stewart-Platform + PhaseSpace + markers)

For 6.3 6.4 experiments: (Acrylic root canal model + truth tooth)

### 6.2 Admittance Control

In order to prove the validation of admittance control, we set up this experiment.

Here we built a Stewart platform, which had six degrees of freedom and provided a slight movement. We used a Stewart platform to simulate a motion of a patient. Basically, when the patient moves to a position, our system should move to the same place. Therefore, we planned to observe the target's and the handpiece's position

to validate that our system can track the patient. Besides, we use PhaseSpace to obtain their motion in real-time. PhaseSpace is a motion capture device whose resolution is around 1 mm. Before starting this experiment, we should fix a relative position between the file and the acrylic tooth. We made the file rotate and get stuck in the root canal of an acrylic model. Then we used "Doctor dragging" mode to install the acrylic model on the Stewart platform. Therefore, we can guarantee that the relative position between the file and the acrylic tooth.

We moved the Stewart platform in horizontal and vertical directions separately. The motion planning in the horizontal direction is a square which is  $10 \times 10$  mm and in the vertical direction is a linear motion from 0 to 40 mm.

### **6.3 Automatically Direction Changing**

Validation of Self-alignment Mode

(Metrics: time, completeness and file breakage)

(Completeness definition: comparison of pixel area before and after experiment via image)

### **6.4 Repetitive Experiment**

validation of repetitive experiment

(Metrics: file breakage, compare with and without reverse)

## **Chapter 7**

### **Conclusions and Future works**

(Patient move tracking via cable, root canals searching)



# Chapter 8

## Appendix

### 8.1 Forward Kinematics

$${}^0_6\mathbf{T} = {}^0_1\mathbf{T} \cdot {}^1_2\mathbf{T} \cdot {}^2_3\mathbf{T} \cdot {}^3_4\mathbf{T} \cdot {}^4_5\mathbf{T} \cdot {}^5_6\mathbf{T} = \begin{bmatrix} {}^0_6\mathbf{R}_{3 \times 3} & {}^0\mathbf{p}_{6\text{org}} \\ 0_{1 \times 3} & 1 \end{bmatrix} = \begin{bmatrix} t_{11} & t_{12} & t_{13} & t_{14} \\ t_{21} & t_{22} & t_{23} & t_{24} \\ t_{31} & t_{32} & t_{33} & t_{34} \\ 0 & 0 & 0 & 1 \end{bmatrix}$$

$$\begin{aligned}
t_{11} &= -S_6(C_4S_1 + S_4(C_1S_3 - C_2 - C_1C_3S_2)) - C_6(C_5(S_1S_4 - C_4(C_1S_3 \\
&\quad - C_2 - C_1C_3S_2)) - S_5(C_1C_3 - C_2 + C_1S_2S_3)) \\
t_{12} &= S_6(C_5(S_1S_4 - C_4(C_1S_3 - C_2 - C_1C_3S_2)) - S_5(C_1C_3 - C_2 + C_1S_2S_3)) \\
&\quad - C_6(C_4S_1 + S_4(C_1S_3 - C_2 - C_1C_3S_2)) \\
t_{13} &= -S_5(S_1S_4 - C_4(C_1S_3 - C_2 - C_1C_3S_2)) - C_5(C_1C_3 - C_2 + C_1S_2S_3) \\
t_{14} &= 135C_1S_2 - 70S_5(S_1S_4 - C_4(C_1S_3 - C_2 - C_1C_3S_2)) - 70C_5(C_1C_3 - C_2 \\
&\quad + C_1S_2S_3) - 120C_1C_3 - C_2 - 120C_1S_2S_3 - 38C_1S_3 - C_2 + 38C_1C_3S_2 \\
t_{21} &= S_6(C_1C_4 + S_4(C_3S_2S_1 - S_1S_3 - C_2)) + C_6(C_5(C_1S_4 - C_4(C_3S_2S_1 \\
&\quad - S_1S_3 - C_2)) + S_5(C_3S_1 - C_2 + S_2S_1S_3)) \\
t_{22} &= C_6(C_1C_4 + S_4(C_3S_2S_1 - S_1S_3 - C_2)) - S_6(C_5(C_1S_4 - C_4(C_3S_2S_1 \\
&\quad - S_1S_3 - C_2)) + S_5(C_3S_1 - C_2 + S_2S_1S_3))
\end{aligned}$$



$$t_{23} = S_5(C_1S_4 - C_4(C_3S_2S_1 - S_1S_3 - C_2)) - C_5(C_3S_1 - C_2 + S_2S_1S_3)$$

$$t_{24} = 135S_2S_1 + 70S_5(C_1S_4 - C_4(C_3S_2S_1 - S_1S_3 - C_2)) - 70C_5(C_3S_1 - C_2 \\ + S_2S_1S_3) + 38C_3S_2S_1 - 120C_3S_1 - C_2 - 120S_2S_1S_3 - 38S_1S_3 - C_2$$

$$t_{31} = C_6(S_5(C_3S_2 - S_3 - C_2) + C_4C_5(C_3 - C_2 + S_2S_3)) - S_4S_6(C_3 - C_2 \\ + S_2S_3)$$

$$t_{32} = -S_6(S_5(C_3S_2 - S_3 - C_2) + C_4C_5(C_3 - C_2 + S_2S_3)) - C_6S_4(C_3 - C_2 \\ + S_2S_3)$$

$$t_{33} = C_4S_5(C_3 - C_2 + S_2S_3) - C_5(C_3S_2 - S_3 - C_2)$$

$$t_{34} = 120S_3 - C_2 - 120C_3S_2 - 38C_3 - C_2 - 38S_2S_3 - 135 - C_2 \\ - 70C_5(C_3S_2 - S_3 - C_2) + 70C_4S_5(C_3 - C_2 + S_2S_3) + 135$$

## 8.2 Jacobian matrix

### 8.2.1 J<sub>g0</sub>

$$\begin{aligned} j_{g0,21} = & 135C_1S_2 - 120C_1S_2S_3 - 70S_1S_4S_5 + 120C_1C_2C_3 + 38C_1C_2S_3 \\ & + 38C_1C_3S_2 + 70C_1C_2C_3C_5 - 70C_1C_5S_2S_3 - 70C_1C_2C_4S_3S_5 \\ & - 70C_1C_3C_4S_2S_5 \end{aligned}$$

$$\begin{aligned} j_{g0,22} = & -S_1(120C_2S_3 - 38C_2C_3 - 135C_2 + 120C_3S_2 + 38S_2S_3 + 70C_2C_5S_3 \\ & + 70C_3C_5S_2 + 70C_2C_3C_4S_5 - 70C_4S_2S_3S_5) \end{aligned}$$

$$\begin{aligned} j_{g0,23} = & -2S_1(60C_2S_3 - 19C_2C_3 + 60C_3S_2 + 19S_2S_3 + 35C_2C_5S_3 \\ & + 35C_3C_5S_2 + 35C_2C_3C_4S_5 - 35C_4S_2S_3S_5) \end{aligned}$$

$$j_{g0,24} = 70S_5(C_1C_4 + C_2S_1S_3S_4 + C_3S_1S_2S_4)$$

$$j_{g0,25} = -70C_5(C_2C_4S_1S_3 - C_1S_4 + C_3C_4S_1S_2) - 70C_{34}S_1S_5$$

$$j_{g0,26} = 0$$

$$j_{g0,31} = 0$$

$$\begin{aligned} j_{g0,32} = & 120S_2S_3 - 120C_2C_3 - 38C_2S_3 - 38C_3S_2 - 135S_2 + 70C_5S_2S_3 \\ & - 70C_2C_3C_5 + 70C_2C_4S_3S_5 + 70C_3C_4S_2S_5 \end{aligned}$$

$$j_{g0,33} = 120S_2S_3 - 38C_2S_3 - 38C_3S_2 - 120C_2C_3 + 70C_5S_2S_3 - 70C_2C_3C_5$$

$$+ 70C_2C_4S_3S_5 + 70C_3C_4S_2S_5$$

$$j_{g0,34} = 70C_{34}S_4S_5$$

$$j_{g0,35} = 70S_{34}S_5 - 70C_{34}C_4C_5$$

$$j_{g0,36} = 0$$

$$j_{g0,41} = \theta_4S_1S_2S_3 - \theta_3C_1 - \theta_5C_1C_4 - \theta_4C_2C_3S_1 - \theta_6C_1S_4S_5 - \theta_2C_1$$

$$- \theta_6C_2C_3C_5S_1 - \theta_5C_2S_1S_3S_4 - \theta_5C_3S_1S_2S_4 + \theta_6C_5S_1S_2S_3$$

$$+ \theta_6C_2C_4S_1S_3S_5 + \theta_6C_3C_4S_1S_2S_5$$

$$j_{g0,42} = \theta_5C_1C_2C_3S_4 - \theta_4C_1C_2S_3 - \theta_4C_1C_3S_2 - S_1 - \theta_6C_1C_2C_5S_3$$

$$- \theta_6C_1C_3C_5S_2 - \theta_5C_1S_2S_3S_4 - \theta_6C_1C_2C_3C_4S_5 + \theta_6C_1C_4S_2S_3S_5$$

$$j_{g0,43} = \theta_5C_1C_2C_3S_4 - \theta_4C_1C_2S_3 - \theta_4C_1C_3S_2 - S_1 - \theta_6C_1C_2C_5S_3$$

$$- \theta_6C_1C_3C_5S_2 - \theta_5C_1S_2S_3S_4 - \theta_6C_1C_2C_3C_4S_5 + \theta_6C_1C_4S_2S_3S_5$$

$$j_{g0,44} = \theta_5(S_1S_4 + C_1C_2C_4S_3 + C_1C_3C_4S_2) - C_1S_2S_3 + C_1C_2C_3$$

$$+ \theta_6S_5(C_1C_2S_3S_4 - C_4S_1 + C_1C_3S_2S_4)$$

$$j_{g0,45} = -C_4S_1 - \theta_6(C_5(S_1S_4 - C_4(C_1S_3 - C_2 - C_1C_3S_2))) - S_5(C_1C_3$$

$$- C_2 + C_1S_2S_3)) - S_4(C_1S_3 - C_2 - C_1C_3S_2)$$

$$j_{g0,46} = C_{34}C_1C_5 - S_5(S_1S_4 + C_1C_2C_4S_3 + C_1C_3C_4S_2)$$

$$j_{g0,51} = \theta_4C_1C_2C_3 - \theta_3S_1 - \theta_5C_4S_1 - \theta_2S_1 - \theta_4C_1S_2S_3 - \theta_6S_1S_4S_5$$

$$+ \theta_6C_1C_2C_3C_5 + \theta_5C_1C_2S_3S_4 + \theta_5C_1C_3S_2S_4 - \theta_6C_1C_5S_2S_3$$

$$- \theta_6C_1C_2C_4S_3S_5 - \theta_6C_1C_3C_4S_2S_5$$

$$j_{g0,52} = C_1 - \theta_4C_2S_1S_3 - \theta_4C_3S_1S_2 + \theta_5C_2C_3S_1S_4 - \theta_6C_2C_5S_1S_3$$

$$- \theta_6C_3C_5S_1S_2 - \theta_5S_1S_2S_3S_4 - \theta_6C_2C_3C_4S_1S_5 + \theta_6C_4S_1S_2S_3S_5$$

$$j_{g0,53} = C_1 - \theta_4C_2S_1S_3 - \theta_4C_3S_1S_2 + \theta_5C_2C_3S_1S_4 - \theta_6C_2C_5S_1S_3$$

$$j_{g0,55} = C_1 C_4 + S_{34} S_1 S_4 - \theta_6 C_{34} S_1 S_5 + \theta_6 C_1 C_5 S_4 - \theta_6 C_2 C_4 C_5 S_1 S_3$$

$$- \theta_6 C_3 C_4 C_5 S_1 S_2$$

$$j_{g0,56} = C_{34} C_5 S_1 - S_5 (C_2 C_4 S_1 S_3 - C_1 S_4 + C_3 C_4 S_1 S_2)$$

$$j_{g0,61} = 1$$

$$j_{g0,62} = \theta_6 S_{34} C_4 S_5 - \theta_6 C_{34} C_5 - \theta_5 S_{34} S_4 - \theta_4 C_{34}$$

$$j_{g0,63} = \theta_6 S_{34} C_4 S_5 - \theta_6 C_{34} C_5 - \theta_5 S_{34} S_4 - \theta_4 C_{34}$$

$$j_{g0,64} = \theta_5 C_2 C_3 C_4 - C_3 S_2 - C_2 S_3 - \theta_5 C_4 S_2 S_3 + \theta_6 C_2 C_3 S_4 S_5 - \theta_6 S_2 S_3 S_4 S_5$$

$$j_{g0,65} = \theta_6 (S_{34} S_5 - C_{34} C_4 C_5) + C_{34} S_4$$

$$j_{g0,66} = - S_{34} C_5 - C_{34} C_4 S_5$$

**8.2.2 Jg6**

$$\begin{aligned}
j_{g6,11} &= 135C_4S_2S_6 + 120C_2C_3C_4S_6 + 70C_2C_3C_6S_4 + 38C_2C_4S_3S_6 \\
&\quad + 38C_3C_4S_2S_6 + 135C_5C_6S_2S_4 - 120C_4S_2S_3S_6 - 70C_6S_2S_3S_4 \\
&\quad - 70C_2S_3S_5S_6 - 70C_3S_2S_5S_6 + 70C_2C_3C_4C_5S_6 + 120C_2C_3C_5C_6S_4 \\
&\quad + 38C_2C_5C_6S_3S_4 + 38C_3C_5C_6S_2S_4 - 70C_4C_5S_2S_3S_6 \\
&\quad - 120C_5C_6S_2S_3S_4 \\
j_{g6,12} &= 70C_4C_6 - 38C_6S_5 - 120S_4S_6 - 70C_5S_4S_6 + 135S_3S_4S_6 + 120C_4C_5C_6 \\
&\quad - 135C_3C_6S_5 - 135C_4C_5C_6S_3 \\
j_{g6,13} &= 70C_4C_6 - 38C_6S_5 - 120S_4S_6 - 70C_5S_4S_6 + 120C_4C_5C_6 \\
j_{g6,14} &= 70S_5S_6 \\
j_{g6,15} &= 70C_6 \\
j_{g6,16} &= 0 \\
j_{g6,21} &= 135C_4C_6S_2 + 120C_2C_3C_4C_6 + 38C_2C_4C_6S_3 + 38C_3C_4C_6S_2 \\
&\quad - 70C_2C_3S_4S_6 - 120C_4C_6S_2S_3 - 70C_2C_6S_3S_5 - 70C_3C_6S_2S_5 \\
&\quad - 135C_5S_2S_4S_6 + 70S_2S_3S_4S_6 + 70C_2C_3C_4C_5C_6 - 120C_2C_3C_5S_4S_6 \\
&\quad - 70C_4C_5C_6S_2S_3 - 38C_2C_5S_3S_4S_6 - 38C_3C_5S_2S_4S_6
\end{aligned}$$

$$+ 120C_5S_2S_3S_4S_6$$

$$j_{g6,22} = 38S_5S_6 - 120C_6S_4 - 70C_4S_6 + 135C_6S_3S_4 + 135C_3S_5S_6$$

$$- 120C_4C_5S_6 - 70C_5C_6S_4 + 135C_4C_5S_3S_6$$

$$j_{g6,23} = 38S_5S_6 - 120C_6S_4 - 70C_4S_6 - 120C_4C_5S_6 - 70C_5C_6S_4$$

$$j_{g6,24} = 70C_6S_5$$

$$j_{g6,25} = -70S_6$$

$$j_{g6,26} = 0$$

# Reference

- [1] “the ministry of health and welfare,” 2018, <https://dep.mohw.gov.tw/dos/cp-1735-3245-113.html>. 1
- [2] “the acadamy of endodontology,” 2021, <http://www.aeroc.org.tw/about/>. 1
- [3] G. Kim, H. Seo, S. Im, D. Kang, and S. Jeong, “A study on simulator of human-robot cooperative manipulator for dental implant surgery,” *2009 IEEE International Symposium on Industrial Electronics*, pp. 2159–2164, 2009. 4
- [4] J. Li, Z. Shen, W. Xu, W. Y. Lam, R. T. C. Hsung, E. H. Pow, K. Kosuge, and Z. Wang, “A compact dental robotic system using soft bracing technique,” *IEEE Robotics and Automation Letters*, vol. 4, pp. 1271–1278, 2019. 4
- [5] “Yomi, neocis,” 2017, <https://www.neocis.com/>. 4
- [6] B. Sattapan, G. J. Nervo, J. E. Palamara, and H. H. Messer, “Defects in rotary nickel-titanium files after clinical use,” *Journal of Endodontics*, vol. 26, no. 3, pp. 161–165, 2000. 5

- [7] M.-K. Wu, D. Barkis, A. Roris, and P. Wesselink, “Does the first file to bind correspond to the diameter of the canal in the apical region?” *International Endodontic Journal*, vol. 35, no. 3, pp. 264–267, 2002. 9
- [8] J. Agrawal, P. K. Shenai, L. Chatra, P. Y. Kumar *et al.*, “Evaluation of normal range of mouth opening using three finger index: South india perspective study,” *Indian Journal of Dental Research*, vol. 26, no. 4, p. 361, 2015. 9
- [9] C. Yang, J. Wang, L. Mi, X. Liu, Y. Xia, Y. Li, S. Ma, and Q. Teng, “A four-point measurement model for evaluating the pose of industrial robot and its influence factor analysis,” *Industrial Robot: An International Journal*, 2017. 21
- [10] T. Tang, H. Lin, Yu Zhao, Wenjie Chen, and M. Tomizuka, “Autonomous alignment of peg and hole by force/torque measurement for robotic assembly,” in *2016 IEEE International Conference on Automation Science and Engineering (CASE)*, 2016, pp. 162–167. 28
- [11] P. Zou, Q. Zhu, J. Wu, and J. Jin, “An approach for peg-in-hole assembling based on force feedback control,” in *2019 Chinese Automation Congress (CAC)*, 2019, pp. 3269–3273. 29